7 SUBLIMATION AND VAPOR DEPOSITION

7.1 Introduction

When the pressure and temperature of ice are above the triple point pressure and temperature of water is heated, melting occurs as discussed in Chapter 6. However, when the ice is exposed to moist air with a partial pressure of water below its triple point pressure, heating of the ice will result in a phase change from ice directly to vapor without first going through the liquid phase. Spacecrafts and space suits can reject heat by sublimating ice into the vacuum of space. Another application for sublimation of ice is the preparation of specimens using freeze-drying for a scanning electronic microscope (SEM) or a transmission electronic microscope (TEM). This type of phase change is referred to as sublimation. The opposite process is deposition, which describes the process of vapor changing directly to solid without going through the condensation and freezing. The phase-change processes related to solids can be illustrated by a phase diagram in Fig. 7.1. Sublimation and deposition will be the subjects of this chapter.

When a subcooled solid is exposed to its superheated vapor, as shown in Fig. 7.2(a), the vapor phase temperature is above the temperature of the solid-vapor interface and the temperature in the solid is below the interfacial temperature. The boundary condition at the solid-vapor interface is

$$k_s \frac{\partial T_s}{\partial x} - h_\delta (T_\infty - T_\delta) = \rho_s h_{sv} \frac{d\delta}{dt} \tag{7.1}$$

where h_δ is the convective heat transfer coefficient at the solid-vapor interface, h_{sv} is the latent heat of sublimation, and δ is the thickness of the sublimable or deposited material. The interfacial velocity $d\delta/dt$ in eq. (7.1) can be either positive or negative, depending on the direction of the overall heat flux at the interface. While a negative interfacial velocity signifies sublimation, a positive interfacial velocity signifies deposition. When the vapor phase is superheated, as shown in Fig. 7.2(a), the solid-vapor interface is usually smooth and stable.

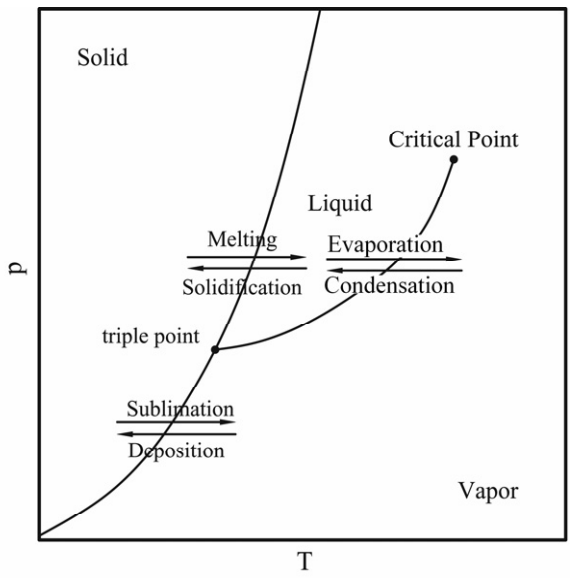

Figure 7.1 Phase diagram for solid-liquid and solid-vapor phase change.

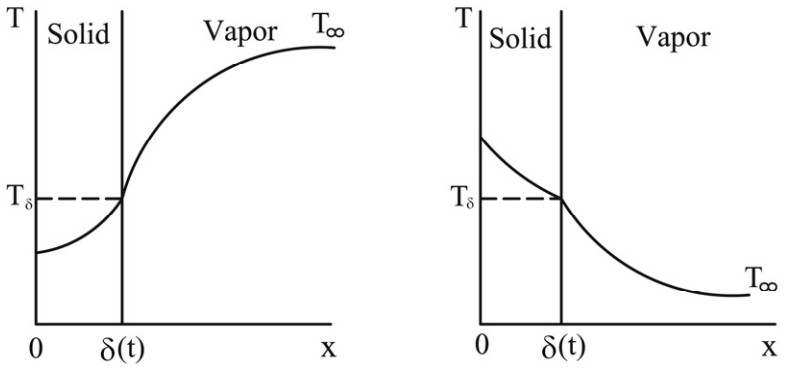

(a) Subcooled solid exposed to superheated vapor

(b) Superheated solid exposed to supercooled vapor

Figure 7.2 Temperature distribution in sublimation and deposition.

In another possible scenario, as shown in Fig. 7.2 (b), the solid temperature is above the interfacial temperature and the vapor phase is supercooled. The interfacial energy balance for this case can still be described by eq. (7.1). Depending on the degrees of superheat in the solid phase and supercooling in the vapor phase [the relative magnitude of the first and second terms in eq. (7.1)], both sublimation and deposition are possible. During sublimation, a smooth and

stable interface can be obtained. During deposition, on the other hand, the interface is dendritic and not stable, because supercooled vapor is not stable. The solid formed by deposition of supercooled vapor has a porous structure. During sublimation or deposition, the latent heat of sublimation can be supplied from or absorbed by either the solid phase or the vapor phase, depending on the temperature distributions in both phases.

Naphthalene sublimation is also a technique whereby a heat transfer coefficient can be obtained through the measurement of a mass transfer coefficient and the analogy between heat and mass transfer (Eckert and Goldstein, 1976). The significant advantages of this method include its high accuracy and the simplicity of the experimental apparatus. In addition, the local heat transfer coefficient can be obtained by measuring the local sublimed depth of the specimen.

Vapor deposition, which finds applications in coating and thermal manufacturing processes, is classified into two broad categories (Seshau, 2001): Physical Vapor Deposition (PVD) and Chemical Vapor Deposition (CVD). PVD operates at a very low pressure and transports the species generated by one of two means: (1) evaporation, or (2) bombarding the target materials to the substrate through free molecular flow or transition flow. CVD, on the other hand, is a process in which material is formed on a substrate by chemical reaction of gaseous precursors using activation energy. The deposited film thickness can range from a few nanometers, as applied to optical coating, to tens of microns, as applied to wear-resistance coating (Jenson *et al.*, 1991). Conventional CVD has been extensively investigated by many researchers and a detailed literature review is given by Mahajan (1996). In a pyrolytic CVD process, the entire substrate is heated and vapor deposition occurs over the whole substrate. When a laser beam is used to heat the substrate, only a very small spot on the substrate is heated by the laser beam and vapor deposition occurs only on the heated spot. In this case the activation energy is provided by the laser beam and it is therefore referred to as Laser Chemical Vapor Deposition (LCVD; Kwok and Chiu, 2003). LCVD can also be based on chemical reactions initiated photolytically, which involves tuning the laser to an electrical or vibrational level of the gas (Bauerle, 1996). The irradiated material decomposes, and the products deposit on the cooler substrate to form the solid film (Mazumder and Kar, 1995).

Section 7.2 presents analytical solutions of sublimation over a flat plate in parallel flow and inside a tube; the problems are treated as a conjugated heat and mass transfer problem. Section 7.2 also includes a detailed analysis of a sublimation process with chemical reaction. Section 7.3 presents an in-depth discussion of CVD, including various CVD configurations, governing equations, transport properties and several selected applications.

7.2 Sublimation

7.2.1 Sublimation over a Flat Plate

Sublimation over a flat plate can find its application in analogy between heat and mass transfer (Kurosaki, 1973; Zhang *et al.*, 1996). Figure 7.3 shows the physical model of the sublimation problem considered by Zhang et al. (1996). A flat plate is coated with a layer of sublimable material and is subject to constant heat flux heating underneath. A gas with the ambient temperature T_∞ and mass fraction of sublimable material ω_∞ flows over the flat plate at a velocity of u_∞. The heat flux applied from the bottom of the flat plate will be divided into two parts: one part is used to supply the latent heat of sublimation, and another part is transferred to the gas through convection. The sublimated vapor is injected into the boundary layer and is removed by the gas flow.

The following assumptions are made in order to solve the problem:

1. The flat plate is very thin, and so the thermal resistance of the flat plate can be neglected.
2. The gas is incompressible, with no internal heat source in the gas.
3. The sublimation problem is two-dimensional steady state.

The governing equations for mass, momentum, energy and species of the problem are

$$\frac{\partial u}{\partial x}+\frac{\partial v}{\partial y}=0 \tag{7.2}$$

$$u\frac{\partial u}{\partial x}+v\frac{\partial u}{\partial y}=\nu\frac{\partial^2 u}{\partial y^2} \tag{7.3}$$

$$u\frac{\partial T}{\partial x}+v\frac{\partial T}{\partial y}=\alpha\frac{\partial^2 T}{\partial y^2} \tag{7.4}$$

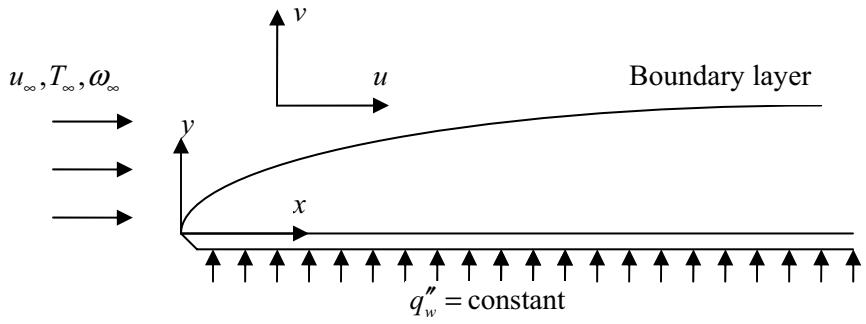

Figure 7.3 Sublimation on a flat plate with constant heat flux.

$$u\frac{\partial \omega}{\partial x}+v\frac{\partial \omega}{\partial y}=D\frac{\partial^2 \omega}{\partial y^2} \tag{7.5}$$

Nonslip condition at the surface of the flat plat require that

$$u=0,\quad y=0 \tag{7.6}$$

For a binary mixture that contains the vapor sublimable substance and gas, the molar flux of the sublimable substance at the surface of the flat plate is [see eq. (1.102)]

$$\dot{m}''=-\frac{\rho D}{1-\omega}\frac{\partial \omega}{\partial y},\quad y=0 \tag{7.7}$$

Since the mass fraction of the sublimable substance in the mixture is very low, i.e., $\omega \ll 1$, the mass flux at the wall can be simplified to

$$\dot{m}''=-\rho D\frac{\partial \omega}{\partial y},\quad y=0 \tag{7.8}$$

Sublimation at the surface causes a normal blowing velocity, $v_w=\dot{m}''/\rho$, at the surface. The normal velocity at the surface of the flat plate is therefore

$$v=v_w=-\rho D\left.\frac{\partial \omega}{\partial y}\right|_{y=0},\quad y=0 \tag{7.9}$$

The energy balance at the surface of the flat plate is

$$-k\frac{\partial T}{\partial y}-\rho h_{sv}D\frac{\partial \omega}{\partial y}=q_w'',\quad y=0 \tag{7.10}$$

Another reasonable, practical, representable boundary condition at the surface of the flat plate emerges by setting the mass fraction at the wall as the saturation mass fraction at the wall temperature. The mass fraction and the temperature at the surface of the flat plate have the following relationship (Kurosaki, 1973, 1974):

$$\omega=aT+b,\quad y=0 \tag{7.11}$$

where a and b are constants that depend on the sublimable material and its temperature.

As $y\to\infty$, the boundary conditions are

$$u\to u_\infty,\ T\to T_\infty,\ \omega\to\omega_\infty \tag{7.12}$$

Introducing the stream function ψ,

$$u=\frac{\partial \psi}{\partial y}\qquad v=-\frac{\partial \psi}{\partial x} \tag{7.13}$$

the continuity equation (7.2) is automatically satisfied, and the momentum equation in terms of the stream function becomes

$$\frac{\partial \psi}{\partial y}\frac{\partial^2 \psi}{\partial x\partial y}-\frac{\partial \psi}{\partial x}\frac{\partial^2 \psi}{\partial y^2}=\nu\frac{\partial^3 \psi}{\partial y^3} \tag{7.14}$$

Similarity solutions for eq. (7.14) do not exist unless the injection velocity v_w is proportional to $x^{1/2}$, and the incoming mass fraction of the sublimable

substance, ω_∞, is equal to the saturation mass fraction corresponding to the incoming temperature T_∞ (Kurosaki, 1974; Zhang *et al.*, 1996). The governing equations cannot be reduced to ordinary differential equations. The local nonsimilarity solution proposed by Zhang *et al.* (1996) will be presented here.

Defining the following similarity variables:

$$\xi = \frac{x}{L}, \quad \eta = y\sqrt{\frac{u_\infty}{2\nu L\xi}}, \quad f = \frac{\psi}{\sqrt{2\nu u_\infty L\xi}}$$
$$\theta = \frac{k(T-T_\infty)}{q''_w\sqrt{2\nu L\xi/u_\infty}}, \quad \varphi = \frac{\rho h_{fv} D(\omega-\omega_\infty)}{q''_w\sqrt{2\nu L\xi/u_\infty}} \tag{7.15}$$

eqs. (7.14) and (7.4) – (7.5) become

$$f''' + ff'' = 2\xi\left(f'F' - f''F\right) \tag{7.16}$$

$$\theta'' + \mathrm{Pr}(f\theta' - f'\theta) = 2\,\mathrm{Pr}\,\xi\left(f'\Theta - \theta' F\right) \tag{7.17}$$

$$\varphi'' + \mathrm{Sc}(f\varphi' - f'\varphi) = 2\,\mathrm{Sc}\,\xi\left(f'\Phi - \varphi' F\right) \tag{7.18}$$

where prime ' represents partial derivative with respect to η, and all upper case variables represent partial derivative of primary similarity variable with respect to ξ.

$$F = \frac{\partial f}{\partial \xi}, \quad \Theta = \frac{\partial \theta}{\partial \xi}, \quad \Phi = \frac{\partial \varphi}{\partial \xi} \tag{7.19}$$

It can be seen from eqs. (7.16) – (7.18) that the similarity solution exists only if F=Θ=Φ=0. In order to use eqs. (7.16) – (7.18) to obtain a solution for the sublimation problem, the supplemental equations about F, Θ, and Φ must be obtained. Taking partial derivatives of eqs. (7.16) – (7.18) with respect to ξ and neglecting the higher order term, one obtains

$$F''' + Ff'' + F''f = 2\left(f'F' - f''F\right) \tag{7.20}$$

$$\Theta'' + \mathrm{Pr}(F\theta' + f\Theta' - F'\theta - f'\Theta) = 2\,\mathrm{Pr}\left(f'\Theta - \theta' F\right) \tag{7.21}$$

$$\Phi'' + \mathrm{Sc}(F\varphi' + f\Phi' - F'\varphi - f'\Phi) = 2\,\mathrm{Sc}\left(f'\Phi - \varphi' F\right) \tag{7.22}$$

The boundary conditions of eqs. (7.16) – (7.18) and eqs. (7.20) – (7.22) are

$$f'(\xi,0) = 0, \quad \eta = 0 \tag{7.23}$$

$$f(\xi,0) = -\frac{2}{3}B\left[\xi^{1/2}\varphi'(\xi,0) - \xi^{3/2}\Phi'(\xi,0)\right], \quad \eta = 0 \tag{7.24}$$

$$f'(\xi,\infty) = 1, \quad \eta = \infty \tag{7.25}$$

$$F'(\xi,0) = 0, \quad \eta = 0 \tag{7.26}$$

$$F(\xi,0) = -\frac{1}{3}B\left[\frac{1}{2}\xi^{-1/2}\varphi'(\xi,0) - \xi^{1/2}\Phi'(\xi,0)\right], \quad \eta = 0 \tag{7.27}$$

$$F'(\xi,\infty) = 0, \quad \eta = \infty \tag{7.28}$$

$$\theta'(\xi,0) + \varphi'(\xi,0) = -1, \quad \eta = 0 \tag{7.29}$$

$$\theta(\xi,\infty) = 0, \quad \eta = \infty \tag{7.30}$$

$$\Theta'(\xi,0) + \Phi'(\xi,0) = 0, \quad \eta = 0 \tag{7.31}$$

$$\Theta(\xi,\infty)=0, \quad \eta=\infty \tag{7.32}$$

$$\varphi(\xi,0)=\frac{ah_{sv}}{c_p}\frac{1}{Le}\theta(\xi,0)+\varphi_s\xi^{-1/2}, \quad \eta=0 \tag{7.33}$$

$$\varphi(\xi,\infty)=0, \quad \eta=\infty \tag{7.34}$$

$$\Phi(\xi,0)=\frac{ah_{sv}}{c_p}\frac{1}{Le}\Theta(\xi,0)-\frac{\varphi_s}{2\xi^{3/2}}, \quad \eta=0 \tag{7.35}$$

$$\Phi(\xi,\infty)=0, \quad \eta=\infty \tag{7.36}$$

where

$$B=\frac{q''_w}{\rho h_{sv}\nu}\sqrt{\frac{2\nu L}{u_\infty}} \tag{7.37}$$

reflects the effect of injection velocity at the surface due to sublimation, and

$$\varphi_s=\frac{\rho h_{sv}D(\omega_{sat,\infty}-\omega_\infty)}{q''_w\sqrt{2\nu L/u_\infty}} \tag{7.38}$$

represents the effect of the mass fraction of the sublimable substance in the incoming flow. $\omega_{sat,\infty}$ is saturation mass fraction corresponding to the incoming temperature:

$$\omega_{sat,\infty}=aT_\infty+b \tag{7.39}$$

The set of ordinary differential equations (7.16) – (7.18) and (7.20) – (7.22) with boundary conditions specified by eqs. (7.23) – (7.36) are boundary value

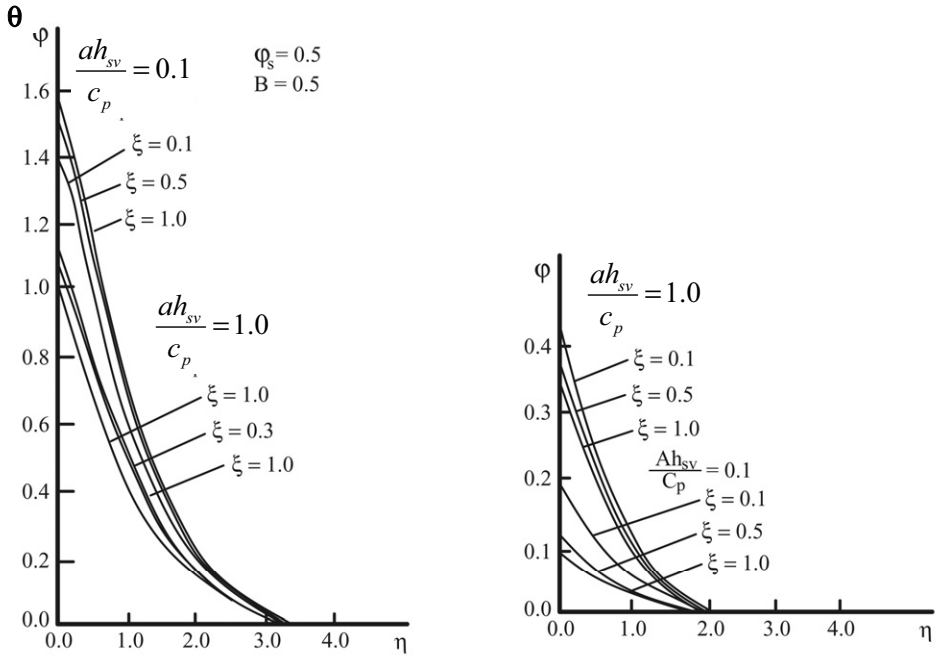

Figure 7.4 Temperature and mass fraction distributions (Zhang *et al.* 1996).

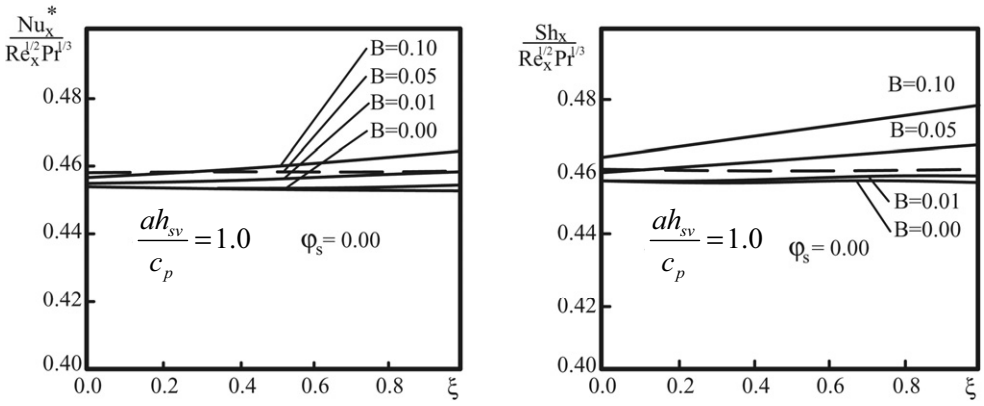

Figure 7.5 Nusselt number based on convection and Sherwood number (Zhang *et al.* 1996).

problems that can be solved using a shooting method (Zhang *et al.*, 1996). Figure 7.4 shows typical dimensionless temperature and mass fraction profiles obtained by numerical solution. It can be seen that the dimensionless temperature and mass fraction at different ξ are also different, which is further evidence that a similarity solution does not exist.

Once the converged solution is obtained, the local Nusselt number based on the *total* heat flux at the bottom of the flat plate is

$$Nu_x = \frac{h_w x}{k} = \frac{[q_w'' /(T_w - T_\infty)]x}{k} = \frac{\mathrm{Re}_x^{1/2}}{\sqrt{2}\theta(\xi,0)} \tag{7.40}$$

and the Nusselt number based on convective heat transfer is

$$Nu_x^* = \frac{h_x x}{k} = \frac{x}{T_w - T_\infty}\left(\frac{\partial T}{\partial y}\right)_{y=0} = -\frac{\theta'(\xi,0)}{\sqrt{2}\theta(\xi,0)}\mathrm{Re}_x^{1/2} \tag{7.41}$$

The Sherwood number is

$$Sh_x = \frac{h_m x}{D} = \frac{x}{\omega_w - \omega_\infty}\left.\frac{\partial \omega}{\partial y}\right|_{y=0} = -\frac{\varphi'(\xi,0)}{\sqrt{2}\varphi\theta(\xi,0)}\mathrm{Re}_x^{1/2} \tag{7.42}$$

Figure 7.5 shows the effect of blowing velocity on the Nusselt number based on convective heat transfer and the Sherwood number for $\varphi_{sat,\infty} = 0$, i.e., the mass fraction of sublimable substance is equal to the saturation mass fraction corresponding to the incoming temperature. It can be seen that the effect of blowing velocity on mass transfer is stronger than that on heat transfer.

7.2.2 Sublimation inside an Adiabatic Tube

In addition to the external sublimation discussed in the preceding subsection, internal sublimation is also very important. Sublimation inside an adiabatic and

externally heated tube will be analyzed in this and the next subsections. The physical model of the problem under consideration is shown in Fig. 7.6 (Zhang and Chen, 1990). The inner surface of a circular tube with radius R is coated with a layer of sublimable material which will sublime when gas flows through the tube. The fully-developed gas enters the tube with a uniform inlet mass fraction of the sublimable substance, ω_0, and a uniform inlet temperature, T_0. Since the outer wall surface is adiabatic, the latent heat of sublimation is supplied by the gas flow inside the tube; this in turn causes the change in gas temperature inside the tube. It is assumed that the flow inside the tube is incompressible laminar flow with constant properties. In order to solve the problem analytically, the following assumptions are made:

1. The entrance mass fraction ω_0 is assumed to be equal to the saturation mass fraction at the entry temperature T_0.
2. The saturation mass fraction can be expressed as a linear function of the corresponding temperature.
3. The mass transfer rate is small enough that the transverse velocity components can be neglected.

The fully-developed velocity profile in the tube is

$$u = 2\bar{u}\left[1-\left(\frac{r}{R}\right)^2\right] \tag{7.43}$$

where $\bar{u}$ is the mean velocity of the gas flow inside the tube.

Neglecting axial conduction and diffusion, the energy and mass transfer equations are

$$ur\frac{\partial T}{\partial x} = \alpha\frac{\partial}{\partial r}\left(r\frac{\partial T}{\partial r}\right) \tag{7.44}$$

$$ur\frac{\partial \omega}{\partial x} = D\frac{\partial}{\partial r}\left(r\frac{\partial \omega}{\partial r}\right) \tag{7.45}$$

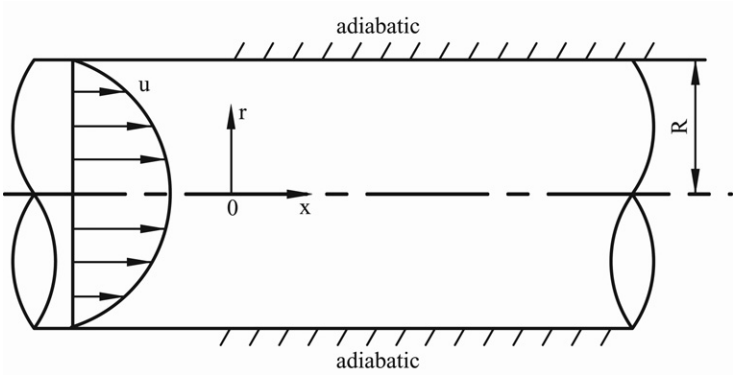

Figure 7.6 Sublimation in an adiabatic tube.

which are subjected to the following boundary conditions:

$$T = T_0, \quad x = 0 \tag{7.46}$$

$$\omega = \omega_0, \quad x = 0 \tag{7.47}$$

$$\frac{\partial T}{\partial r} = \frac{\partial \omega}{\partial r} = 0, \quad r = 0 \tag{7.48}$$

$$-k\frac{\partial T}{\partial r} = \rho D h_{sv}\frac{\partial \omega}{\partial r}, \quad r = R \tag{7.49}$$

Equation (7.49) implies that the latent heat of sublimation is supplied as the gas flows inside the tube. Another boundary condition at the tube wall is obtained by setting the mass fraction at the wall as the saturation mass fraction at the wall temperature (Kurosaki, 1973). According to the second assumption, the mass fraction and temperature at the inner wall have the following relationship:

$$\omega = aT + b, \quad r = R \tag{7.50}$$

where a and b are constants.

The following nondimensional variables are then introduced:

$$\eta = \frac{r}{R} \quad \xi = \frac{x}{R\mathrm{Pe}} \quad \mathrm{Le} = \frac{\alpha}{D} \quad \mathrm{Re} = \frac{2\bar{u}R}{\nu}$$
$$\mathrm{Pe} = \frac{2\bar{u}R}{\alpha} \quad \theta = \frac{T - T_f}{T_0 - T_f} \quad \varphi = \frac{\omega - \omega_f}{\omega_0 - \omega_f} \tag{7.51}$$

where T_f and ω_f are temperature and mass fraction of the sublimable substance, respectively, after heat and mass transfer are fully developed. Equations (7.44) – (7.50) then become

$$\eta(1-\eta^2)\frac{\partial \theta}{\partial \xi} = \frac{\partial}{\partial \eta}\left(\eta\frac{\partial \theta}{\partial \eta}\right) \tag{7.52}$$

$$\eta(1-\eta^2)\frac{\partial \varphi}{\partial \xi} = \frac{1}{Le}\frac{\partial}{\partial \eta}\left(\eta\frac{\partial \varphi}{\partial \eta}\right) \tag{7.53}$$

$$\theta = \varphi = 1, \quad \xi = 0 \tag{7.54}$$

$$\frac{\partial \theta}{\partial \eta} = \frac{\partial \varphi}{\partial \eta} = 0, \quad \eta = 0 \tag{7.55}$$

$$-\frac{\partial \theta}{\partial \eta} = \frac{1}{Le}\frac{\partial \varphi}{\partial \eta}, \quad \eta = 1 \tag{7.56}$$

$$\varphi = \left(\frac{a h_{sv}}{c_p}\right)\theta, \quad \eta = 1 \tag{7.57}$$

The heat and the mass transfer equations (7.52) and (7.53) are independent but their boundary conditions are coupled by eqs. (7.56) and (7.57). The solution of eqs. (7.52) and (7.53) can be obtained via separation of variables. It is assumed that the solution of θ can be expressed as a product of the function of η and a function of ξ, i.e.,

$$\theta = \Theta(\eta)\Gamma(\xi) \tag{7.58}$$

Substituting eq. (7.58) into eq. (7.52), the energy equation becomes

$$\frac{\Gamma'}{\Gamma} = \frac{\dfrac{d}{d\eta}\left(\dfrac{d\Theta}{d\eta}\right)}{\eta(1-\eta^2)\Theta} = -\beta^2 \tag{7.59}$$

where β is the eigenvalue for the energy equation.

Equation (7.59) can be rewritten as the following two ordinary differential equations:

$$\Gamma' + \beta^2\Gamma = 0 \tag{7.60}$$

$$\frac{d}{d\eta}\left(\frac{d\Theta}{d\eta}\right) + \beta^2\eta(1-\eta^2)\Theta = 0 \tag{7.61}$$

The solution of eq. (7.60) is

$$\Gamma = C_1 e^{-\beta^2\xi} \tag{7.62}$$

The boundary condition of eq. (7.61) at $\eta = 0$ is

$$\Theta'(0) = 0 \tag{7.63}$$

The dimensionless temperature is then

$$\theta = C_1\Theta(\eta)e^{-\beta^2\xi} \tag{7.64}$$

Similarly, the dimensionless mass fraction is

$$\varphi = C_2\Phi(\eta)e^{-\gamma^2\xi} \tag{7.65}$$

where γ is the eigenvalue for the conservation of species equation, and $\Phi(\eta)$ satisfies

$$\frac{d}{d\eta}\left(\frac{d\Phi}{d\eta}\right) + Le\gamma^2\eta(1-\eta^2)\Phi = 0 \tag{7.66}$$

and the boundary condition of eq. (7.66) at $\eta = 0$ is

$$\Phi'(0) = 0 \tag{7.67}$$

Substituting eqs. (7.64) – (7.65) into eqs. (7.56) – (7.57), one obtains

$$\beta = \gamma \tag{7.68}$$

$$-\left(\frac{Ah_{sv}}{c_p}\right)\frac{\Theta(1)}{\Phi(1)} = Le\frac{\Theta'(1)}{\Phi'(1)} \tag{7.69}$$

To solve eqs. (7.61) and (7.66) using the Runge-Kutta method it is necessary to specify two boundary conditions for each. However, there is only one boundary condition for each: eqs. (7.63) and (7.67), respectively. Since both eqs. (7.61) and (7.66) are homogeneous, one can assume that the other boundary conditions are $\Theta(0) = \Phi(0) = 1$ and solve for eq. (7.61) and (7.66) numerically. It is necessary to point out that the eigenvalue, β, is still unknown at this point and must be obtained by eq. (7.69). There will be a series of β which satisfy eq. (7.69), and for each value of the β_n there is one set of corresponding Θ_n and Φ_n functions $(n = 1, 2, 3, \cdots)$.

If we use any one of the eigenvalue β_n and corresponding eigen functions – Θ_n and Φ_n – in eqs. (7.64) and (7.65), the solutions of eq. (7.52) and (7.53) become

$$\theta = C_1 \Theta_n(\eta) e^{-\beta_n^2 \xi} \tag{7.70}$$

$$\varphi = C_2 \Phi_n(\eta) e^{-\beta_n^2 \xi} \tag{7.71}$$

which satisfy all boundary conditions except those at $\xi = 0$. In order to satisfy boundary conditions at $\xi = 0$, one can assume that the final solutions of eqs. (7.52) and (7.53) are

$$\theta = \sum_{n=1}^{\infty} G_n \Theta_n(\eta) e^{-\beta_n^2 \xi} \tag{7.72}$$

$$\varphi = \sum_{n=1}^{\infty} H_n \Phi_n(\eta) e^{-\beta_n^2 \xi} \tag{7.73}$$

where G_n and H_n can be obtained by substituting eqs. (7.72) and (7.73) into eq. (7.54), i.e.,

$$1 = \sum_{n=1}^{\infty} G_n \Theta_n(\eta) \tag{7.74}$$

$$1 = \sum_{n=1}^{\infty} H_n \Phi_n(\eta) \tag{7.75}$$

Due to the orthogonal nature of the eigeinfunctions Θ_n and Φ_n, expressions of G_n and H_n can be obtained by

$$G_n = \frac{\int_0^1 \eta(1-\eta^2)\Theta_n(\eta)d\eta + \left[\frac{\Theta_n(1)}{\Phi_n(1)}\right] \int_0^1 \eta(1-\eta^2)\Phi_n(\eta)d\eta}{\int_0^1 \eta(1-\eta^2)\left\{\Theta_n^2(\eta) + \left(Ah_{sv}/c_p\right)\left[\frac{\Theta_n(1)}{\Phi_n(1)}\right]^2 \Phi_n^2(\eta)\right\} d\eta} \tag{7.76}$$

$$H_n = \frac{Ah_{sv}}{c_p} \frac{\Theta_n(1)}{\Phi_n(1)} G_n \tag{7.77}$$

The Nusselt number due to convection and Sherwood number are

$$Nu = \frac{-k \left.\frac{\partial T}{\partial r}\right|_{r=R}}{\bar{T} - T_w} \frac{2R}{k} = -\frac{2}{\bar{\theta} - \theta_w} \sum_{n=1}^{\infty} G_n e^{-\beta_n^2 \xi} \Theta_n'(1) \tag{7.78}$$

$$Sh = \frac{-D \left.\frac{\partial \omega}{\partial r}\right|_{r=R}}{\bar{\omega} - \omega_w} \frac{2R}{D} = -\frac{2}{\bar{\varphi} - \varphi_w} \sum_{n=1}^{\infty} H_n e^{-\beta_n^2 \xi} \Phi_n'(1) \tag{7.79}$$

where $\bar{T}$ and $\bar{\omega}$ are mean temperature and mean mass fraction in the tube.

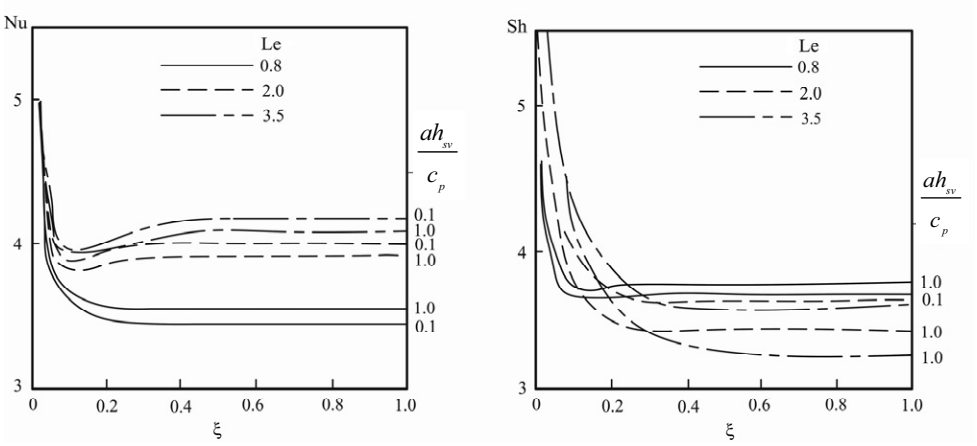

Figure 7.7 Nusselt and Sherwood numbers for sublimation inside an adiabatic tube (Zhang and Chen, 1990).

Figure 7.7 shows heat and mass transfer performance during sublimation inside an adiabatic tube. For all cases, both Nusselt and Sherwood numbers become constant when ξ is greater than a certain number, thus indicating that heat and mass transfer in the tube have become fully developed. The length of the entrance flow increases with increasing Lewis number. While the fully-developed Nusselt number increases with increasing Lewis number, the Sherwood number decreases with increasing Lewis number, because a larger Lewis number indicates larger thermal diffusivity or low mass diffusivity. The effect of (Ah_{sv}/c_p) on Nusselt and Sherwood numbers is relatively insignificant: both Nusselt and Sherwood numbers increase with increasing (Ah_{sv}/c_p) for Le < 1, but increasing (Ah_{sv}/c_p) for Le > 1 results in decreasing Nusselt and Sherwood numbers.

7.2.3 Sublimation inside a Tube Subjected to External Heating

When the outer wall of a tube with a sublimable-material-coated inner wall is heated by a uniform heat flux q'' (see Fig. 7.8), the latent heat will be supplied by part of the heat flux at the wall. The remaining part of the heat flux will be used to heat the gas flowing through the tube. The problem can be described by eqs. (7.43) – (7.50), except that the boundary condition at the inner wall of the tube is replaced by

$$\rho h_{sv} D \frac{\partial \omega}{\partial r} + k \frac{\partial T}{\partial r} = q'' \tag{7.80}$$

where the thermal resistance of the tube wall is neglected because the tube wall and the coated layer are very thin.

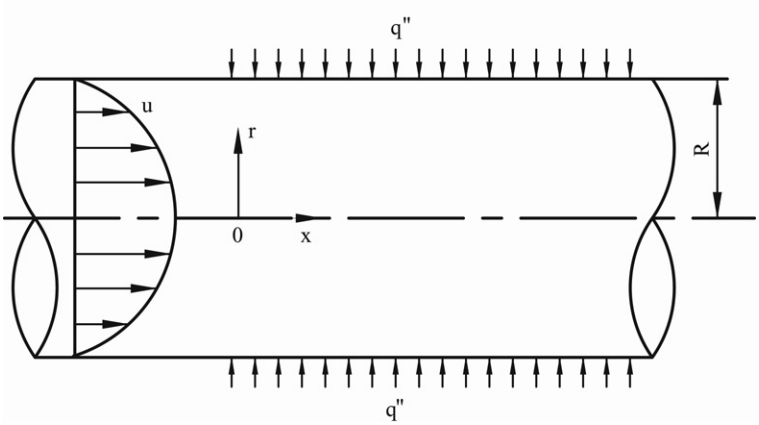

Figure 7.8 Sublimation in a tube heated by a uniform heat flux.

The governing equations for sublimation inside a tube heated by a uniform heat flux can be nondimensionalized by using the dimensionless variables defined in eq. (7.51), except the following:

$$\theta = \frac{k(T - T_0)}{q'' R} \quad \varphi = \frac{h_{sv}(\omega - \omega_{sat,0})}{c_p q'' R} \tag{7.81}$$

where $\omega_{sat,0}$ is the saturation mass fraction corresponding to the inlet temperature T_0, and the resultant dimensionless governing equations and boundary conditions are

$$\eta(1-\eta^2)\frac{\partial \theta}{\partial \xi} = \frac{\partial}{\partial \eta}\left(\eta \frac{\partial \theta}{\partial \eta}\right) \tag{7.82}$$

$$\eta(1-\eta^2)\frac{\partial \varphi}{\partial \xi} = \frac{1}{Le}\frac{\partial}{\partial \eta}\left(\eta \frac{\partial \varphi}{\partial \eta}\right) \tag{7.83}$$

$$\theta = 0, \quad \xi = 0 \tag{7.84}$$

$$\varphi = \varphi_0, \quad \xi = 0 \tag{7.85}$$

$$\frac{\partial \theta}{\partial \eta} = \frac{\partial \varphi}{\partial \eta} = 0, \quad \eta = 0 \tag{7.86}$$

$$\frac{\partial \theta}{\partial \eta} + \frac{1}{Le}\frac{\partial \varphi}{\partial \eta} = 1, \quad \eta = 1 \tag{7.87}$$

$$\varphi = \left(\frac{a h_{sv}}{c_p}\right)\theta, \quad \eta = 1 \tag{7.88}$$

where $\varphi_0 = k h_{sv}(\omega - \omega_{sat,0})/(c_p q'' R)$ in eq. (7.85).

The sublimation problem under consideration is not homogeneous, because eq. (7.87) is a nonhomogeneous boundary condition. The solution of the problem is consistent with its particular (fully developed) solution and the solution of the corresponding homogeneous problem (Zhang and Chen, 1992), i.e.,

$$\theta(\xi,\eta)=\theta_1(\xi,\eta)+\theta_2(\xi,\eta) \tag{7.89}$$

$$\varphi(\xi,\eta)=\varphi_1(\xi,\eta)+\varphi_2(\xi,\eta) \tag{7.90}$$

While the fully developed solutions of temperature and mass fraction, $\theta_1(\xi,\eta)$ and $\varphi_1(\xi,\eta)$, respectively, must satisfy eqs. (7.82) – (7.83) and (7.86) – (7.88), the corresponding homogeneous solutions of the temperature and mass fraction – $\theta_2(\xi,\eta)$ and $\varphi_2(\xi,\eta)$ – must satisfy eqs. (7.82), (7.83), (7.86), and (7.88), as well as the following conditions:

$$\theta_2=-\theta_1(0,\eta),\quad \xi=0 \tag{7.91}$$

$$\varphi_2=\varphi_0-\varphi_1(\xi,\eta),\quad \xi=0 \tag{7.92}$$

$$\frac{\partial\theta_2}{\partial\eta}+\frac{1}{Le}\frac{\partial\varphi_2}{\partial\eta}=0,\quad \eta=1 \tag{7.93}$$

The fully developed profiles of the temperature and mass fraction are

$$\theta_1=\frac{1}{1+ah_{sv}/c_p}\left[4\xi+\eta^2\left(1-\frac{1}{4}\eta^2\right)+\varphi_0 +\frac{11\text{Le}\ ah_{sv}/c_p-18ah_{sv}/c_p-7}{24(1+ah_{sv}/c_p)}\right] \tag{7.94}$$

$$\varphi_1=\frac{ah_{sv}/c_p}{1+ah_{sv}/c_p}\left[4\xi+Le\eta^2\left(1-\frac{1}{4}\eta^2\right)+\varphi_0 -\frac{7\text{Le}\ ah_{sv}/c_p+18Le-11}{24(1+ah_{sv}/c_p)}\right] \tag{7.95}$$

The solution of the corresponding homogeneous problem can be obtained by separation of variables:

$$\theta_2=\sum_{n=1}^{\infty}G_n\Theta_n(\eta)e^{-\beta_n^2\xi} \tag{7.96}$$

$$\varphi_2=\sum_{n=1}^{\infty}H_n\Phi_n(\eta)e^{-\beta_n^2\xi} \tag{7.97}$$

where

$$G_n=\frac{\int_0^1\eta(1-\eta^2)\theta_2(0,\eta)\Theta_n(\eta)d\eta+\left[\frac{\Theta_n(1)}{\Phi_n(1)}\right]\int_0^1\eta(1-\eta^2)\varphi_2(0,\eta)\Phi_n(\eta)d\eta}{\int_0^1\eta(1-\eta^2)\left\{\Theta_n^2(\eta)+\left(ah_{sv}/c_p\right)\left[\frac{\Theta_n(1)}{\Phi_n(1)}\right]^2\Phi_n^2(\eta)\right\}d\eta} \tag{7.98}$$

$$H_n=\frac{ah_{sv}}{c_p}\frac{\Theta_n(1)}{\Phi_n(1)}G_n \tag{7.99}$$

and β_n is the eigenvalue of the corresponding homogeneous problem.

The Nusselt number based on the total heat flux at the external wall is

$$Nu = \frac{2q''R}{k(T_w - \bar{T})} = \frac{2}{\theta_w - \bar{\theta}}$$

$$= \frac{2(1 + Ah_{sv}/c_p)}{\frac{11}{24} + \left(1 + \frac{ah_{sv}}{c_p}\right)\sum_{n=1}^{\infty} G_n e^{-\beta_n^2 \xi}\left[\Theta_n(1) + \frac{4}{\beta_n^2}\Theta_n'(1)\right]} \tag{7.100}$$

where θ_w and $\bar{\theta}$ are dimensionless wall and mean temperatures, respectively.

The Nusselt number based on the convective heat transfer coefficient is

$$Nu^* = \frac{2h_x R}{k} = \frac{2R}{T_w - \bar{T}}\left(\frac{\partial T}{\partial r}\right)_{r=R} = \frac{2}{\theta_w - \bar{\theta}}\left(\frac{\partial \theta}{\partial \eta}\right)_{\eta=1}$$

$$= \frac{2 + 2(1 + ah_{sv}/c_p)\sum_{n=1}^{\infty} G_n e^{-\beta_n^2 \xi}\Theta_n'(1)}{\frac{11}{24} + \left(1 + \frac{ah_{sv}}{c_p}\right)\sum_{n=1}^{\infty} G_n e^{-\beta_n^2 \xi}\left[\Theta_n(1) + \frac{4}{\beta_n^2}\Theta_n'(1)\right]} \tag{7.101}$$

The Sherwood number is

$$Sh = \frac{2h_{m,x}R}{D} = \frac{2R}{\omega_w - \bar{\omega}}\frac{\partial \omega}{\partial r}\bigg|_{r=R} = \frac{2}{\varphi_w - \bar{\varphi}}\frac{\partial \varphi}{\partial \eta}\bigg|_{\eta=1}$$

$$= \frac{2Le\frac{ah_{sv}}{c_p} + 2(1 + \frac{ah_{sv}}{c_p})\sum_{n=1}^{\infty} H_n e^{-\beta_n^2 \xi}\Phi_n'(1)}{\frac{11}{24}Le\frac{ah_{sv}}{c_p} + \left(1 + \frac{ah_{sv}}{c_p}\right)\sum_{n=1}^{\infty} G_n e^{-\beta_n^2 \xi}\left[\Phi_n(1) + \frac{4}{\beta_n^2 Le}\Phi_n'(1)\right]} \tag{7.102}$$

When the heat and mass transfer are fully developed, eqs. (7.100) – (7.102) reduce to

$$Nu = \left(1 + \frac{ah_{sv}}{c_p}\right)\frac{48}{11} \tag{7.103}$$

$$Nu^* = \frac{48}{11} \tag{7.104}$$

$$Sh = \frac{48}{11} \tag{7.105}$$

The variations of the local Nusselt number based on total heat flux along the dimensionless location ξ are shown in Fig. 7.9. It is evident from Fig. 7.9(a) that Nu increases significantly with increasing (Ah_{sv}/c_p). The Lewis number has very little effect on Nu_x when $(Ah_{sv}/c_p) = 0.1$, but its effects become obvious in the region near the entrance when $(Ah_{sv}/c_p) = 1.0$ and gradually diminishes in the region near the exit. The effect of φ_0 on Nu, as is seen from Fig. 7.9(b), has

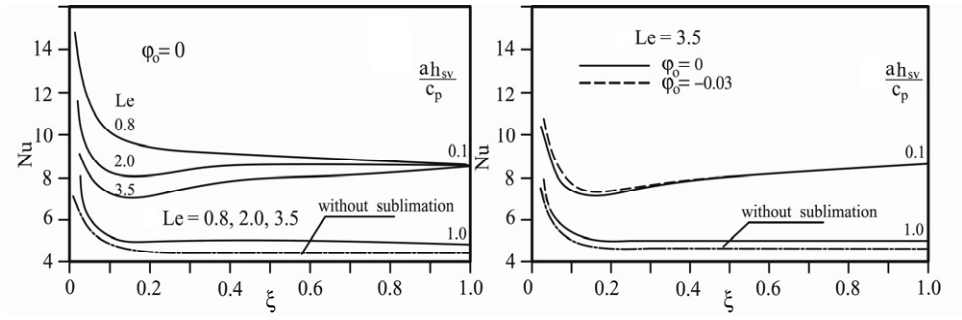

(a) $\varphi_0 = 0$ (b) Le=3.5

Figure 7.9 Nusselt number based on total heat flux

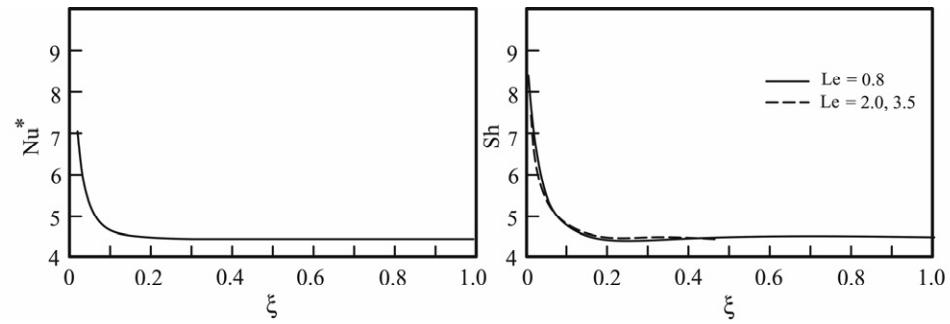

Figure 7.10 Nusselt number based on convective heat flux and Sherwood number.

no apparent influence in almost the entire region when (Ah_{sv}/c_p) = 1.0. When $(Ah_{sv}/c_p) = 0.1$, Nu_x increases slightly when ξ is small.

The variation of the local Nusselt number based on convective heat flux, Nu^*, is shown in Fig. 7.10(a). Only a single curve is obtained, which implies that Nu^* remains unchanged when the mass transfer parameters are varied. The value of Nu^* is exactly the same as for the process without sublimation. Figure 7.10(b) shows the Sherwood number for various parameters. It is evident that (Ah_{sv}/c_p) and φ_0 have no effect on Sh_x, but Le has an insignificant effect on Sh_x in the entry region.

Example 7.1 Air flows through a circular tube that has a radius of R and is heated by external convection. The external convection heat transfer coefficient and fluid temperature are h_e and T_e, respectively. The inner surface of the tube is coated by a layer of sublimable material. The fluid with a mass fraction of sublimable substance ω_0 and a temperature T_0 enters the tube with a velocity U. For the sake of simplicity, the flow inside the tube is assumed to be slug flow (uniform velocity). The heat and mass transfer inside the tube are assumed to be developing. Find the

Nusselt number based on total heat transfer and convective heat transfer, as well as the Sherwood number. The thermal diffusivity and mass diffusivity is assumed to be the same, i.e., Le = 1.

Solution: The physical model of the problem is shown in Fig. 7.11, and the conservations of energy and species equations are

$$Ur\frac{\partial T}{\partial x}=\alpha\frac{\partial}{\partial r}\left(r\frac{\partial T}{\partial r}\right) \tag{7.106}$$

$$Ur\frac{\partial \omega}{\partial x}=D\frac{\partial}{\partial r}\left(r\frac{\partial \omega}{\partial r}\right) \tag{7.107}$$

with the following boundary conditions:

$$T=T_0,\quad x=0 \tag{7.108}$$

$$\omega=\omega_0,\quad x=0 \tag{7.109}$$

$$\frac{\partial T}{\partial r}=\frac{\partial \omega}{\partial r}=0,\quad r=0 \tag{7.110}$$

$$k\frac{\partial T}{\partial r}+\rho D h_{sv}\frac{\partial \omega}{\partial r}=h_e(T_e-T),\quad r=R \tag{7.111}$$

Introducing the following nondimensional variables,

$$\eta=\frac{r}{R}\quad \xi=\frac{x}{RPe}\quad Pe=\frac{2UR}{\alpha}\quad Bi=\frac{h_eR}{k}$$
$$\theta=\frac{T_e-T}{T_e-T_0}\qquad \varphi=\frac{\omega_e-\omega}{\omega_e-\omega_0}\quad \omega_e=aT_e+b \tag{7.112}$$

where ω_e is the saturation mass fraction corresponding to T_e, the governing equations become

$$\frac{\eta}{2}\frac{\partial \theta}{\partial \xi}=\frac{\partial}{\partial \eta}\left(\eta\frac{\partial \theta}{\partial \eta}\right) \tag{7.113}$$

$$\frac{\eta}{2}\frac{\partial \varphi}{\partial \xi}=\frac{\partial}{\partial \eta}\left(\eta\frac{\partial \varphi}{\partial \eta}\right) \tag{7.114}$$

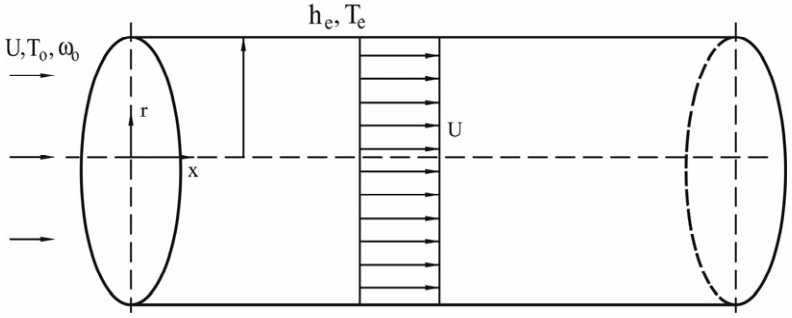

Figure 7.11 Sublimation in a tube heated by external convection.

$$\theta = \varphi = 1, \quad \xi = 0 \tag{7.115}$$

$$\frac{\partial \theta}{\partial \eta} = \frac{\partial \varphi}{\partial \eta} = 0, \quad \eta = 0 \tag{7.116}$$

$$\frac{Ah_{sv}}{c_p}\frac{\partial \theta}{\partial \eta} + \frac{\partial \varphi}{\partial \eta} = -Bi\theta_w, \quad \eta = 1 \tag{7.117}$$

$$\varphi_w = \theta_w, \quad \eta = 1 \tag{7.118}$$

Equations (7.113) and (7.114) can be solved using separation of variables, and the resulting temperature and mass fraction distributions are (Zhang, 2002)

$$\theta = \varphi = \sum_{n=1}^{\infty} \frac{2J_1(\beta_n)J_0(\beta_n \eta)}{\beta_n \left[J_0^2(\beta_n) + J_1^2(\beta_n) \right]} e^{-\beta_n^2 \xi} \tag{7.119}$$

where J_0 and J_1 are the zeroth and first order Bessel functions.

The Nusselt number based on the total heat supplied by the external fluid is

$$Nu = \frac{2R}{k}\frac{h_e(T_e - T_w)}{(T_w - \bar{T})} = \frac{2Bi\theta_w}{\bar{\theta} - \theta_w} \tag{7.120}$$

The Nusselt number based on the heat transferred to the fluid inside the tube is

$$Nu^* = -\frac{2R}{(T_w - \bar{T})}\left(\frac{\partial T}{\partial r}\right)_{r=R} = \frac{2}{\bar{\theta} - \theta_w}\left(\frac{\partial \theta}{\partial \eta}\right)_{\eta=1} \tag{7.121}$$

The Sherwood number is

$$Sh = -\frac{2R}{\omega_w - \bar{\omega}}\left(\frac{\partial \omega}{\partial r}\right)_{r=R} = \frac{2}{\bar{\varphi} - \varphi_w}\left(\frac{\partial \varphi}{\partial \eta}\right)_{\eta=1} \tag{7.122}$$

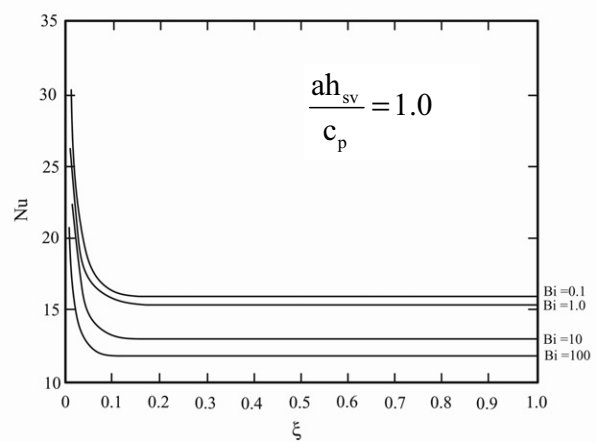

Figure 7.12 Effect of Biot number on Nu $(ah_{sv}/c_p = 1)$.

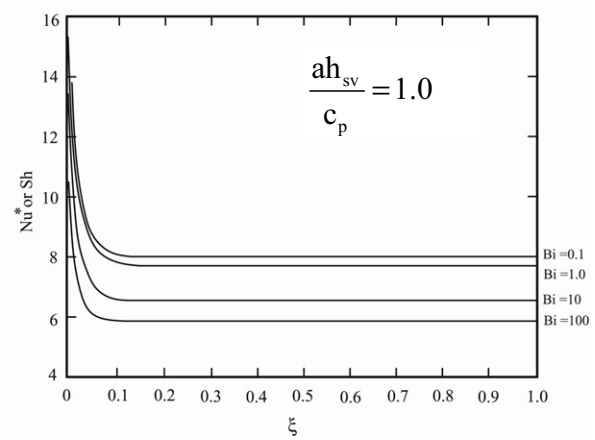

Figure 7.13 Effect of Biot number on Nu^* or Sh $(ah_{sv}/c_p = 1)$.

The Nusselt number based on the heat transferred to the fluid inside the tube and the Sherwood number are identical, since $\theta = \varphi$ as indicated by eq. (7.119). Fig. 7.12 shows the variation of local Nusselt number based on total heat supplied from the fluid outside the tube. The dimensionless lengths ofthe entrance slightly increase with decreasing Biot number, and the dimensionless lengths of entrance are approximately equal to 0.1. Nusselt numbers become constants after ξ is greater than 0.1. The fully-developed Nusselt number increases with decreasing Biot number. Fig. 7.13 shows the variation of local Nusselt number based on heat transferred to the fluid inside the tube or local Sherwood number. The variations of Nu^* and Sh are similar to that of Nu in Fig. 7.12.

7.2.4 Sublimation with Chemical Reaction

During combustion involving a solid fuel, the solid fuel may burn directly or it may be sublimated before combustion. In the latter case – which will be discussed in this subsection – gaseous fuel diffuses away from the solid-vapor surface. Meanwhile, the gaseous oxidant diffuses toward the solid-vapor interface. Under the right conditions, the mass flux of vapor fuel and the gaseous oxidant meet and the chemical reaction occurs at a certain zone known as the flame. The flame is usually a very thin region with a color dictated by the temperature of combustion.

Figure 7.14 shows the physical model of the problem under consideration (Kaviany, 2001). The concentration of the fuel is highest at the solid fuel surface, and decreases as the location of the flame is approached. The gaseous fuel diffuses away from the solid fuel surface and meets the oxidant as it flows parallel to the solid fuel surface. Combustion occurs in a thin reaction zone where

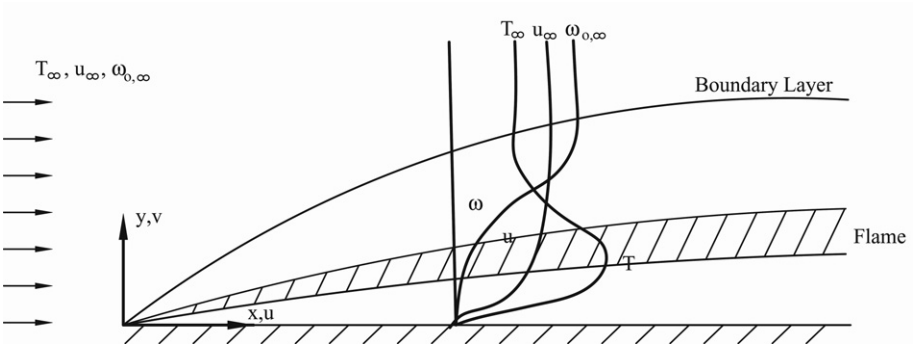

Figure 7.14 Sublimation with chemical reaction.

the temperature is the highest, and the latent heat of sublimation is supplied by combustion. The combustion of solid fuel through sublimation can be modeled as a steady-state boundary layer type flow with sublimation and chemical reaction.

To model the problem, the following assumptions are made:

1. The fuel is supplied by sublimation at a steady rate.
2. The Lewis number is unity, so the thermal and concentration boundary layers have the same thickness.
3. The buoyancy force is negligible.

The conservations of mass, momentum, energy and species of mass in the boundary layer are

$$\frac{\partial(\rho u)}{\partial x}+\frac{\partial(\rho v)}{\partial y}=0 \tag{7.123}$$

$$u\frac{\partial u}{\partial x}+v\frac{\partial u}{\partial y}=\frac{\partial}{\partial y}\left(\nu\frac{\partial u}{\partial y}\right) \tag{7.124}$$

$$\frac{\partial}{\partial x}(\rho c_p uT)+\frac{\partial}{\partial y}(\rho c_p vT)=\frac{\partial}{\partial y}\left(k\frac{\partial T}{\partial y}\right)+\dot{m}_o'''h_{c,o} \tag{7.125}$$

$$\frac{\partial}{\partial x}(\rho u\omega_o)+\frac{\partial}{\partial y}(\rho v\omega_o)=\frac{\partial}{\partial y}\left(\rho D\frac{\partial\omega_o}{\partial y}\right)-\dot{m}_o''' \tag{7.126}$$

where $\dot{m}_o'''$ is rate of oxidant consumption (kg/m^3-s). $h_{c,o}$ is the heat released by combustion per unit mass consumption of the oxidant (J/kg), which is different from the combustion heat defined in Chapter 3. ω_o is mass fraction of the oxidant in the gaseous mixture.

The corresponding boundary conditions of eqs. (7.123) – (7.126) are

$$u\to u_\infty,\quad T\to T_\infty,\quad \omega_o\to\omega_{o,\infty}\ \text{ at }\ y\to\infty \tag{7.127}$$

$$u = 0, \quad v = \frac{\dot{m}_f''}{\rho}, \quad \frac{\partial \omega_o}{\partial y} = 0 \text{ at } y = 0 \tag{7.128}$$

where $\dot{m}_f''$ is the rate of solid fuel sublimation per unit area (kg/m^2-s) and ρ is the density of the mixture.

The shear stress at the solid fuel surface is

$$\tau_w = \mu \frac{\partial u}{\partial y}, \quad y = 0 \tag{7.129}$$

The heat flux at the solid fuel surface is

$$q_w'' = -k \frac{\partial T}{\partial y}, \quad y = 0 \tag{7.130}$$

The exact solution of the heat and mass problem described by eqs. (7.123) – (7.126) can be obtained using conventional numerical simulation, which is very complex. However, it is useful here to introduce the results obtained by Kaviany (2001) using analogy between momentum and heat transfer. Multiplying eq. (7.126) by $h_{c,o}$ and adding the result to eq. (7.125), one obtains

$$\begin{aligned} &\frac{\partial}{\partial x}\left[\rho u(c_p T + \omega_o h_{c,o})\right] + \frac{\partial}{\partial y}\left[\rho v(c_p T + \omega_o h_{c,o})\right] \\ &= \frac{\partial}{\partial y}\left[k \frac{\partial T}{\partial y} + \rho D h_{c,o} \frac{\partial \omega_o}{\partial y}\right] \end{aligned} \tag{7.131}$$

Considering the assumption that Lewis number is unity, i.e., $Le = \alpha / D = 1$, eq. (7.131) can be rewritten as

$$\begin{aligned} &\frac{\partial}{\partial x}\left[\rho u(c_p T + \omega_o h_{c,o})\right] + \frac{\partial}{\partial y}\left[\rho v(c_p T + \omega_o h_{c,o})\right] \\ &= \frac{\partial}{\partial y}\left[\rho \alpha \frac{\partial}{\partial y}(c_p T + \omega_o h_{c,o})\right] \end{aligned} \tag{7.132}$$

which can be viewed as an energy equation with quantity $c_p T + \omega_o h_{c,o}$ as a dependent variable.

Since $\partial \omega_o / \partial y = 0$ at $y = 0$, i.e., the solid fuel surface is not permeable for the oxidant, eq. (7.130) can be rewritten as

$$q_w'' = -\rho \alpha \frac{\partial}{\partial y}(c_p T + \omega_o h_{c,o}), \quad y = 0 \tag{7.133}$$

Analogy between surface shear stress and the surface energy flux yields

$$\begin{aligned} q_w'' &= \frac{\tau_w}{u_\infty}\left[(c_p T + \omega_o h_{c,o})_w - (c_p T + \omega_o h_{c,o})_\infty\right] \\ &= \frac{\tau_w}{u_\infty}\left[c_p (T_w - T_\infty) + h_{c,o}(\omega_{o,w} - \omega_{o,\infty})\right] \end{aligned} \tag{7.134}$$

The energy balance at the surface of the solid fuel is

$$-q''_w = \dot{m}''_f h_{sv} + q''_\ell \tag{7.135}$$

where the two terms on the right-hand side of eq. (7.135) represent the latent heat of sublimation, and the sensible heat required to raise the surface temperature of the solid fuel to sublimation temperature and heat loss to the solid fuel.

Combining eqs. (7.134) and (7.135) yields the rate of sublimation on the solid fuel surface

$$\dot{m}''_f = Z \frac{\tau_w}{u_\infty} \tag{7.136}$$

where Z is transfer driving force or transfer number defined as

$$Z = \frac{c_p (T_\infty - T_w) + h_{c,o} (\omega_{o,\infty} - \omega_{o,w})}{h_{sg} + q''_\ell / m''_f} \tag{7.137}$$

By using the friction coefficient –

$$C_f = \frac{\tau_w}{\rho u_\infty^2 / 2} \tag{7.138}$$

eq. (7.136) becomes

$$\dot{m}''_f = \frac{C_f}{2} \rho u_\infty Z \tag{7.139}$$

The surface blowing velocity of the gaseous fuel is then

$$v_w = \frac{\dot{m}''_f}{\rho} = \frac{C_f}{2} u_\infty Z \tag{7.140}$$

where the friction coefficient C_f can be obtained from the solution of boundary layer flow over a flat plate with blowing on the surface (Kaviany, 2001; Kays *et al.*, 2004). The similarity solution of the boundary layer flow problem exists only if blowing velocity satisfies $v_w \propto x^{-1/2}$. In this case, one can define a blowing parameter as

$$B = \frac{(\rho v)_w}{(\rho u)_\infty} \mathrm{Re}_x^{1/2} \tag{7.141}$$

Combination of eqs. (7.140) and (7.141) yields

$$B = \frac{Z}{2} \mathrm{Re}_x^{1/2} C_f \tag{7.142}$$

Glassman (1987) recommended an empirical form of eq. (7.142) based on numerical and experimental results:

$$B = \frac{\ln(1+Z)}{2.6 Z^{0.15}} \tag{7.143}$$

Example 7.2 Air with a temperature of 27 °C flows at 1 m/s over a 1-m long solid fuel surface with a temperature of 727 °C. The concentration of the oxidant at the solid fuel surface is 0.1, and the heat released per unit mass of the oxidant consumed is 12000 kJ/kg. The latent heat of sublimation for the solid fuel is 1500 kJ/kg. Neglect the sensible heat required to raise

the surface temperature of the solid fuel to sublimation temperature, and heat loss to the solid fuel. Estimate the average blowing velocity due to sublimation on the fuel surface.

Solution: The mass fractions of the oxygen at the solid fuel surface and in the incoming air are, respectively, $\omega_{o,w} = 0.1$ and $\omega_{o,\infty} = 0.21$. The specific heat of gas, approximately taken as specific heat of air at $T_{ave} = (T_w + T_\infty)/2 = 377$ °C, is c_p=1.063 kJ/kg-K. The combustion heat per unit oxidant consumed is $h_{c,o} = 12000$ kJ/kg. The latent heat of sublimation is $h_{sv} = 1500$ kJ/kg. The density at the wall and the incoming temperatures are respectively $\rho_w = 0.3482$ kg/m^3 and $\rho_\infty = 1.1614$ kg/m^3. The viscosity at T_{ave} is $\nu = 60.21\times10^{-6}$ m^2/s.

The transfer driving force can be obtained from eq. (7.137), i.e.,

$$Z = \frac{c_p(T_\infty - T_w) + h_{c,o}(\omega_{o,\infty} - \omega_{o,w})}{h_{sv}}$$

$$= \frac{1.063\times(27-727) + 12000\times(0.21-0.1)}{500} = 0.5257$$

The blowing parameter obtained from eq. (7.143) is

$$B = \frac{\ln(1+Z)}{2.6Z^{0.15}} = \frac{\ln(1+0.5257)}{2.6\times0.5257^{0.15}} = 0.1789$$

The blowing velocity at the surface is obtained from eq.(7.141):

$$v_w = \frac{\rho_\infty}{\rho_w} B u_\infty \mathrm{Re}_x^{-1/2} = \frac{\rho_\infty}{\rho_w} B\left(u_\infty \nu\right)^{1/2} x^{-1/2}$$

which can be integrated to yield the average blowing velocity:

$$\overline{v}_w = \frac{2\rho_\infty}{\rho_w} B\left(u_\infty \nu L\right)^{1/2}$$

$$= \frac{2\times1.1614}{0.3482}\times0.1789\times\left(1\times60.21\times10^{-6}\times1\right)^{1/2} = 0.009259\text{m/s}$$

7.3 Chemical Vapor Deposition (CVD)

7.3.1 Introduction

CVD is widely used to fabricate semiconductor devises. It depends on availability of a volatile gaseous chemical that can be converted to solid film through some thermally activated chemical reaction. Chemical Vapor Deposition can be used to produce a large variety of thin films with different precursors. It is very crucial that the chemical reaction takes place on the substrate surface

only, so that a thin film can be deposited onto the substrate. If undesired chemical reactions occur in the gas phase, the solid particles can be formed which may fall onto the substrate or coat the chamber walls. To avoid the undesired chemical reaction, the substrate surface temperature, deposition time, pressure, and surface specificity should be carefully selected. The chemical reaction during a CVD process is usually accomplished in several steps. The path of chemical reactions can be altered by changing the substrate temperature. For example, when titanium tetrabromide ($TiBr_4$) is used as a precursor to deposit titanium film, the chemical reaction is accomplished in the following steps (Mazumder and Kar, 1995):

$$TiBr_4(g) \rightarrow TiBr_2(s)+Br_2(g)$$

$$3TiBr_2(s) \rightarrow 2TiBr(s)+TiBr_4(g)$$

$$4TiBr(g) \rightarrow 3Ti(s)+TiBr_4(g)$$

The mechanisms of chemical reactions for many CVD processes are not clear, so the chemical reactions occurring in a CVD process are often represented by a single overall chemical reaction equation. Table 7.1 summarizes some examples of the overall chemical reactions occurring in CVD processes (including LCVD).

Table 7.1 Overall chemical reaction of CVD processes (including LCVD)

Thin films	Overall reaction	Temperature of reaction	References
Al_2O_3	$Al(l) + H_2O(g) = AlO(g) + H_2(g)$ $AlO(g) + H_2O(g) = Al_2O_3(s) + H_2(g)$	1230-1255°C	Powell *et al.* (1966)
C	$C_xH_y(g)=xC(s)+(y/2)H_2(g)$	700-1450°C	Taylor *et al.* (2004)
GaAs	$GaCI(g) + (1/4)As4(g) = GaAs(s) + HCI(g)$		Sivaram (1995)
GaAs	$GaAs(g) + HCI(g)$ $=GaCI(g) + 1/4(As_4(g)) + 1/2(H_2(g))$	700-850°C	Sivaram (1995)
	$Ga(CH_3)_3+AsH_3 = GaAs+3CH_4$ $Al(CH_3)_3+AsH_3 = AlAs+3CH$	500-800°C	Ueda (1996)
GaN	$Ga(g) + NH_3 = GaN(s) + (3/2)H_2(g)$	650°C	Elyukhin *et al.* (2002)
Ge(s)	$GeH_4 =Ge(s) + 2H_2$		Herring (1990)
Si	$SiH_4(g)=Si(s)+2H_2(g)$	>600°C (polysilicon) >850-900°C (single crystal)	Herring (1990)
SiC	$Si(CH_3)_4(g)=SiC(s)+3CH_4(g)$	700-1450 °C	Sun *et al.* (1998)
SiO_2	$SiH_4+ O_2 = SiO_2 + 2H_2$		Sivaram (1995)
	$SiH_4 + 2N_2O = SiO_2 + 2H_2O + 2N_2$	800°C	Sivaram (1995)
	$SiH_2Cl_2 + 2N_2O = SiO_2 + 2HCI + 2N_2$	> 900°C	Sivaram (1995)
TiO_2	$TiCl_4(g)+O_2(g)=TiO_2(S)+2Cl_2(g)$		Jakubenas *et al.* (1997)
TiN	$TiCl_4(g)+2H_2(g)+(1/2)N_2(g)=TiN(s)+4HCl(g)$	900°C	Mazumder and Kar (1995)

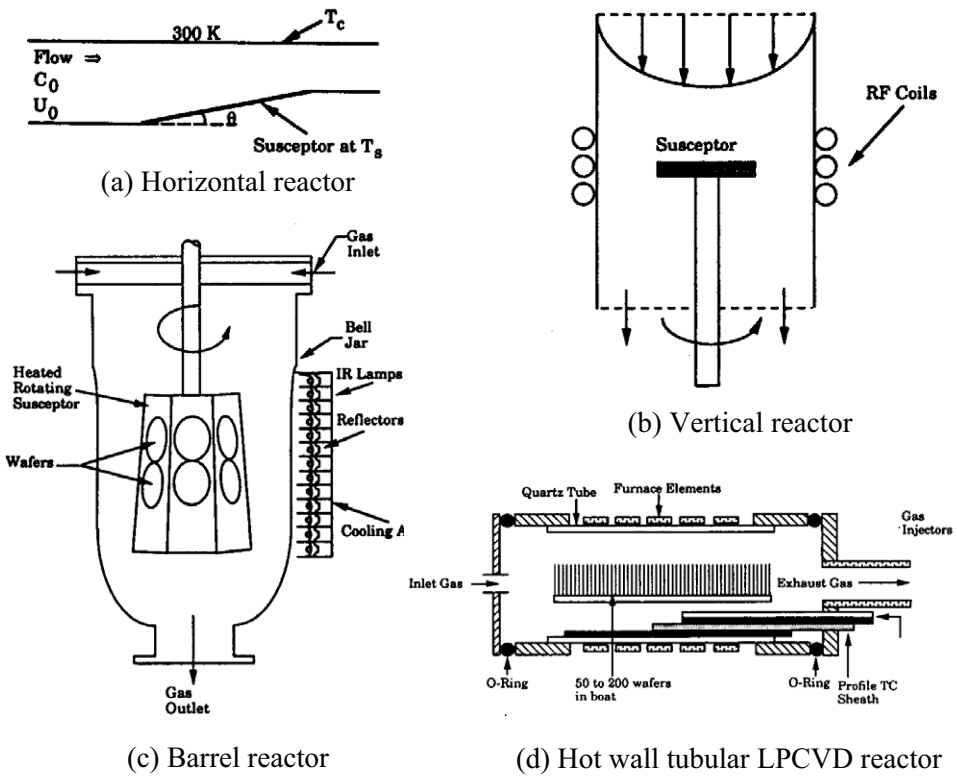

Figure 7.15 Common CVD reactors (Mahajan, 1996; Reprinted with permission from Elsevier)

CVD reactors may operate at atmospheric reduced pressure (APCVD) – which varies from 0.1 to 1 atm – or at low pressure (LPCVD). The typical pressure for LPCVD is 10^{-3} atm. A wide variety of CVD reactors have been developed for its various applications; some of them are illustrated in Fig. 7.15 (Jensen *et al.*, 1991; Mahajan, 1996). The horizontal reactor shown in Fig. 7.15(a) is one of the most established configurations: a rectangular duct. The wafers to be coated are placed on a heated susceptor that is tilted by about 3° in order to ensure uniformity of deposition (Mahajan, 1996). The horizontal reactor is primarily used in CVD research and epitaxial growth of silicon semiconductors (Jensen *et al.*, 1991). In the vertical reactor shown in Fig. 7.15(b), the precursors are injected into a slowly-rotating susceptor on which CVD takes place (Evans and Greif, 1987). The barrel reactor shown in Fig. 7.15(c) is frequently used for large volume production of silicon epitaxial wafers. The wafers sit in shallow pockets on a slightly tapered, slowly rotating heated susceptor. In the CVD reactors shown in Figs. 7.15 (a), (b) and (c), the activation energy for chemical reaction is supplied directly to the susceptors, and the walls are either unheated or cooled. The CVD reactor shown in Fig. 7.15(d), however, is a hot wall tubular reactor that is heated from outside; it is commonly used to deposit polycrystalline

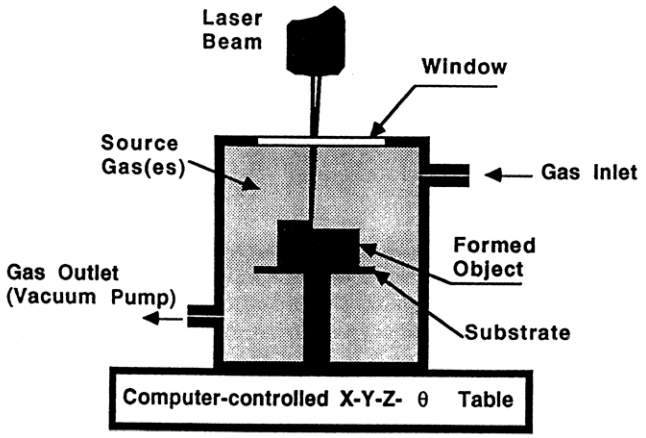

Figure 7.16 SALD system (Marcus et al., 1993).

silicon and other dielectric films. The reactor operates at a low pressure (0.1 to 10 Torr) and is nearly at isothermal condition, with temperatures ranging from 300 to 900 °C (Jensen *et al.*, 1991). In addition to gaseous precursors discussed above, the precursor for CVD can also be liquid as reported by Versteeg et al. (1995).

Figure 7.16 shows a reaction chamber for the Selective Area Laser Deposition (SALD) process (Marcus *et al.*, 1993). In contrast to conventional CVD, in which the entire susceptor is heated, only a very small spot on the substrate is heated by a directed laser beam. Scanning of the substrate surface is accomplished by a movable table. After the first layer of the solid is deposited, consecutive layers can be deposited to build the three-dimensional part based on the CAD design. The pressure inside the chamber is usually under 1 atm and the temperature of the spot under laser irradiation can range from 700 to 1500 °C. Successful deposition of various ceramic and metallic materials using various gaseous precursors has been reported.

7.3.2 Governing Equations of CVD

Since the velocity of the precursors is generally very low and the characteristic length is also very small, the corresponding Reynolds number is under 100 and the Grashof number governing natural convection is under 10^6. Therefore, the transport phenomena in the CVD process are laminar in nature. The temperature in a reactor varies significantly (typically from 300 to 900K), so the Boussinesq approximation is no longer appropriate. It is necessary to use the compressible model for transport phenomena in CVD processes.

The governing equations for the CVD process can be obtained by simplifying the generalized governing equations in Chapter 3. The following assumptions can be made to obtain the governing equations:

1. The reference frame is stationary.
2. The body force **X** is gravitational force, which is the same for all components in the precursors.
3. Dilute approximation is valid because the partial pressure of the reactant is much lower than that of the carrier gas.
4. The deposited film is very thin (from nanometers to microns) and its effect on the flow field can be neglected.

The continuity equation is

$$\frac{D\rho}{Dt} + \rho\nabla\cdot\mathbf{V} = 0 \tag{7.144}$$

where the precursor gases are treated as a compressible fluid mixture.

The momentum equation is

$$\rho\frac{D\mathbf{V}}{Dt} = \nabla\cdot\boldsymbol{\tau}' + \rho\mathbf{g} \tag{7.145}$$

where the stress tensor is

$$\boldsymbol{\tau}' = -p\mathbf{I} + 2\mu\mathbf{D} - \frac{2}{3}\mu(\nabla\cdot\mathbf{V})\mathbf{I} \tag{7.146}$$

The energy equation is

$$\rho c_p\frac{DT}{Dt} = \nabla\cdot(k\nabla T) + T\beta\frac{Dp}{Dt} \tag{7.147}$$

where the effect of viscous dissipation and the Dufour effect have been neglected.

The conservation of species mass in terms of the mass fraction is

$$\rho\frac{D\omega_i}{Dt} = -\nabla\cdot\mathbf{J}_i + \dot{m}_i''', \quad i = 1,2,...N-1 \tag{7.148}$$

where ω_i is the mass fraction of the i^{th} component in the gaseous precursor. The mass flux $\mathbf{J}_i$ includes mass fluxes due to ordinary diffusion driven by the concentration gradient, and thermal (Soret) diffusion. It can be obtained using the approach described in Section 1.3.1. The production rate of the i^{th} species, $\dot{m}_i'''$, can be obtained by analyzing the chemical reaction. If the number of chemical reactions taking place in the system is N_g, the mass production rate is (Mahajan, 1996)

$$\dot{m}_i''' = \sum_{j=1}^{N_g} a_{ij}^g M_i \Re_j^g \tag{7.149}$$

where a_{ij}^g is the stoichiometric coefficient for the i^{th} component in the j^{th} chemical reaction in the gas phase, and $\Re_j^g$ is the net reaction rate of the j^{th} chemical reaction in the gas phase (see Section 3.2.2).

The density of the gas is related to the pressure and temperature by the ideal gas law:

$$\rho = \frac{p}{R_g T} \tag{7.150}$$

The boundary conditions for the governing equations of a CVD process depend on the geometric configuration of the reactor. It is generally assumed that the nonslip condition is applicable to all solid walls. The normal velocity on a solid wall is zero (no penetration) for all walls except the susceptor where chemical reaction takes place. The total net mass flux of all species can lead to a normal velocity component on the susceptor as (Mahajan, 1996)

$$v_n = \frac{1}{\rho} \sum_{i=1}^{N} \sum_{j=1}^{N_s} a_{ij}^s M_i \Re_j^s \tag{7.151}$$

where a_{ij}^s is the stoichiometric coefficient for the i^{th} component in the j^{th} chemical reaction on the susceptor surface, and $\Re_j^g$ is the net reaction rate of the j^{th} chemical reaction on the susceptor surface.

The net surface reaction rate $\Re_j^g$ is a product of the sticking coefficient γ_j (fraction of product that can be stuck on the substrate) and the effusive flux of the j^{th} species (Mahajan, 1996), i.e.,

$$\Re_j^s = \gamma_j \frac{x_j p_j}{\sqrt{2\pi M_j RT}} \tag{7.152}$$

The growth rate of the deposit on the susceptor is

$$\frac{d\delta}{dt} = M_f \sum_{i=1}^{N} \sum_{j=1}^{N_s} a_{ij}^s \Re_j^s \alpha_{i,f} \tag{7.153}$$

where M_f is the molecular mass of the deposited film, and $\alpha_{i,f}$ is the number of film atoms in the i^{th} species.

7.3.3 Transport Properties

The thermophysical properties of various gaseous precursors are necessary to utilize the transport models outlined above. Since the temperature varies significantly throughout a CVD system, the transport phenomena must be modeled using variable thermal physical properties. This requires knowledge of the dependence of the thermophysical properties on temperature. The thermophysical properties of the commonly used gas(es) in CVD are tabulated in Table 7.2.

The viscosity and thermal conductivity of some precursors that are not readily available can be estimated using the method recommended by Bird *et al.* (2002). The viscosity is

$$\mu = 2.6693 \times 10^{-6} \frac{\sqrt{MT}}{\sigma^2 \Omega_\mu} \tag{7.154}$$

Table 7.2 Transport properties of the common gas(es) for CVD (Mahajan, 1996)

Properties	Gas(es)	c_0	c_1	c_2
μ^a (N-s/m²)	TMGa	-1.15×10^{-6}	3.35×10^{-8}	-6.68×10^{-12}
	AsH_3	-4.32×10^{-7}	5.94×10^{-8}	-1.46×10^{-11}
	H_2	2.63×10^{-6}	2.22×10^{-8}	-5.19×10^{-12}
	N_2	4.93×10^{-6}	4.55×10^{-8}	-1.08×10^{-11}
	SiH_4	1.47×10^{-6}	3.66×10^{-8}	-6.81×10^{-12}
k^a (W/m-K)	TMGa	-3.52×10^{-3}	3.85×10^{-5}	-3.84×10^{-8}
	AsH_3	-7.16×10^{-3}	6.53×10^{-5}	-3.47×10^{-9}
	H_2	5.77×10^{-2}	4.43×10^{-4}	-7.54×10^{-8}
	N_2	8.15×10^{-3}	6.24×10^{-5}	-4.48×10^{-9}
	SiH_4	-2.12×10^{-2}	1.45×10^{-4}	-1.31×10^{-8}
c_p^a (kJ/Kg-K)	TMGa	5.40×10^{2}	1.60	0
	AsH_3	2.45×10^{2}	1.08×10^{0}	-4.24×10^{-4}
	H_2	1.44×10^{4}	-2.61×10^{-1}	8.67×10^{-4}
	N_2	1.03×10^{3}	4.58×10^{-3}	1.34×10^{-4}
	SiH_4	4.74×10^{2}	3.26	-1.08×10^{-3}
D_{12}^b (m^2/s)	SiH_4, N_2	-9.64×10^{-1}	6.25×10^{-3}	8.50×10^{-6}
	SiH_4, H_2	-2.90	2.06×10^{-2}	2.81×10^{-5}
	N_2, H_2	-3.20	2.44×10^{-2}	3.37×10^{-5}
	TMGa, H_2	-1.87	1.64×10^{-2}	3.13×10^{-5}
	TMGa, N_2	-4.17×10^{-1}	2.89×10^{-3}	4.93×10^{-6}
	AsH_3, H_2	-2.26	1.73×10^{-2}	2.80×10^{-5}
	AsH_3, N_2	-6.15×10^{-1}	4.57×10^{-3}	7.49×10^{-6}
	TMGa, AsH_3	-2.26×10^{-1}	1.27×10^{-3}	3.18×10^{-6}
k_{12}^T c	H_2,SiH_4	-2.74×10^{-1}	-1.70	-6.35×10^{-3}
	N_2,SiH_4	-5.15×10^{-2}	-1.69	-4.94×10^{-3}
	H_2,N_2	-2.71×10^{-1}	-1.61	-9.15×10^{-3}
	TMGa, H_2	1.32	-1.54	-3.57×10^{-3}
	TMGa, N_2	6.36×10^{-1}	-1.58	-3.36×10^{-3}
	AsH_3,H2	8.86×10^{-1}	-1.57	-4.35×10^{-3}
	AsH_3, N2	3.09×10^{-1}	-1.55	-4.06×10^{-3}
	TMGa, AsH_3	1.94×10^{-1}	-1.79	-1.91×10^{-3}

[a] $\mu, k, c_p = c_0 + c_1 T + c_2 T^2$; [b] $D_{12} = D_{21} = \left(c_0 + c_1 T + c_2 T^2\right)/p$; [c] $k_{12}^T = -k_{12}^T = c_0 x_1 x_2 \left[1 + c_1 \exp(c_2 T)\right]$, for $x_1 \to 0$.

T is absolute temperature (K); Reprinted with permission from Elsevier.

where M is the molecular mass and σ is the collision diameter (Å= 10^{-10} m) of the molecule that can be estimated by

$$\sigma = 0.841 \overline{v}_c^{1/3} \tag{7.155}$$

or

$$\sigma = 1.166 \overline{v}_{b,liq}^{1/3} \tag{7.156}$$

where $\overline{v}_c$ and $\overline{v}_{b,liq}$ are the specific volumes (cm^3/mol) of the precursor at critical point, and of the saturated liquid at normal boiling point, respectively.

The collision integral Ω_μ in eq. (7.154) is a slowly-varying function of dimensionless temperature, $k_b T/\varepsilon$, and is tabulated in Table 7.3. k_b is the

Boltzmann constant and ε is a characteristic energy of interaction between molecules which can be estimated by

$$\frac{\varepsilon}{k_b} = 0.77T_c \tag{7.157}$$

or

$$\frac{\varepsilon}{k_b} = 1.15T_b \tag{7.158}$$

where T_c and T_b are critical temperature and normal boiling point, respectively.

The thermal conductivity of the polyatomic gas is related to its viscosity by

$$k = \left(c_p + \frac{5}{4} R_g \right) \mu \tag{7.159}$$

where R_g is the gas constant.

Table 7.3 Dependence of collision integral Ω_μ on dimensional temperature k_bT/ε (Bird *et al.*, 2002)[a]

k_bT/ε	Ω_μ	$\Omega_{D,12}$	k_bT/ε	Ω_μ	$\Omega_{D,12}$	k_bT/ε	Ω_μ	$\Omega_{D,12}$
0.30	2.840	2.649	1.70	1.249	1.141	4.2	0.9598	0.8748
0.35	2.676	2.468	1.75	1.235	1.128	4.3	0.9551	0.8703
0.40	2.531	2.314	1.80	1.222	1.117	4.4	0.9506	0.8659
0.45	2.401	2.182	1.85	1.209	1.105	4.5	0.9462	0.8617
0.50	2.284	2.066	1.90	1.198	1.095	4.6	0.9420	0.8576
0.55	2.178.	1.965	1.95	1.186	1.085	4.7	0.9380	0.8537
0.60	2.084	1.877	2.00	1.176	1.075	4.8	0.9341	0.8499
0.65	1.999	1.799	2.10	1.156	1.058	4.9	0.9304	0.8463
0.70	1.922	1.729	220	1.138	1.042	5.0	0.9268	0.8428
0.75	1.853	1.667	2.30	1.122	1.027	6.0	0.8962	0.8129
0.80	1.790	1.612	2.40	1.107	1.013	7.0	0.8727	0.7898
0.85	1.734	1.562	2.50	1.0933	1.0006	8.0	0.8538	0.7711
0.90	1.682	1.517	2.60	1.0807	0.9890	9.0	0.8380	0.7555
0.95	1.636	1.477	2.7	1.0691	0.9782	10.0	0.8244	0.7422
1.00	1.593	1.440	2.8	1.0583	0.9682	12.0	0.8018	0.7202
1.05	1.554	1.406	2.9	1.0482	0.9588	14.0	0.7836	0.7025
1.10	1.518	1.375	3.0	1.0388	0.9500	16.0	0.7683	0.6878
1.15	1.485	1.347	3.1	1.0300	0.9418	18.0	0.7552	0.6751
1.20	1.455	1.320	3.2	1.0217	0.9340	20.0	0.7436	0.6640
1.25	1.427	1.296	3.3	1.0139	0.9267	25.0	0.7198	0.6414
1.30	1.401	1.274	3.4	1.0066	0.9197	30.0	0.7010	0.6235
1.35	1.377	1.253	3.5	0.9996	0.9131	35.0	0.6854	0.6088
1.40	1.355	1.234	3.6	0.9931	0.9068	40.0	0.6723	0.5964
1.45	1.334	1.216	3.7	0.9868	0.9008	50.0	0.6510	0.5763
1.50	1.315	1.199	3.8	0.9809	0.8952	75.0	0.6140	0.5415
1.55	1.297	1.183	3.9	0.9753	0.8897	100.0	0.5887	0.5180
1.60	1.280	1.168	4.0	0.9699	0.8845			
1.65	1.264	1.154	4.1	0.9647	0.8796			

[a] Reproduced with permissions from John Wiley and Sons, Limited.

For a mixture of different gases, as is usually the case in CVD processes, the viscosity and the thermal conductivity of the mixture are related to those of the individual components by

$$\mu = \sum_{i=1}^{N} \frac{x_i \mu_i}{\sum_{j=1}^{N} x_i \phi_{ij}} \tag{7.160}$$

$$k = \sum_{i=1}^{N} \frac{x_i k_i}{\sum_{j=1}^{N} x_i \phi_{ij}} \tag{7.161}$$

where

$$\phi_{ij} = \frac{1}{\sqrt{8}} \left(1 + \frac{M_i}{M_j} \right)^{-1/2} \left[1 + \left(\frac{\mu_i}{\mu_j} \right)^{1/2} \left(\frac{M_j}{M_i} \right)^{1/4} \right]^2 \tag{7.162}$$

The specific heat of the gaseous mixture is related to those of the individual components by

$$c_p = \sum_{i=1}^{N} x_i c_{p,i} \tag{7.163}$$

For applications that involve unknown mass diffusivity, it can be estimated by

$$D_{12} = 1.8583 \times 10^{-7} \frac{\sqrt{T^3 \left(M_1^{-1} + M_2^{-1} \right)}}{p \sigma_{12}^2 \Omega_{D,12}} \tag{7.164}$$

where the unit for pressure is atm and

$$\sigma_{12} = \frac{1}{2} \left(\sigma_1 + \sigma_2 \right) \tag{7.165}$$

$\Omega_{D,12}$ is a function of $k_b T / \varepsilon_{12}$ that can be obtained from Table 7.3 using

$$\varepsilon_{12} = \sqrt{\varepsilon_1 \varepsilon_2} \tag{7.166}$$

The concentration of the reactant is usually much lower than that of the carrier gas(es). When the reactant is a single gas diluted by the carrier gas, the diffusivity of the reactant to the carrier gaseous mixture is of interest. If the reactant is defined as component 1 in the precursor, and the carrier gases are components 2 through *N*, the diffusivity of the reactant – 1 – to the carrier gas mixture – *m* – can be obtained by

$$\frac{1 - x_1}{D_{1m}} = \sum_{j=2}^{N} \frac{x_j}{D_{1j}} \tag{7.167}$$

Example 7.3 Titanium tetrachloride ($TiCl_4$) is used as a reactant to deposit titanium nitride, TiN (Zhang and Faghri, 2000). The boiling point of $TiCl_4$ is 136.4 °C, and its liquid specific volume at normal boiling point is 109.7 cm^3/mol. Its specific heat at 900 K is 560.92 J/kg-k. Estimate its viscosity and thermal conductivity at 900 K.

Solution: The molecular mass of $TiCl_4$ is M = 189.71 kg/kmol. The collision diameter of $TiCl_4$ is obtained from eq. (7.156):

$$\sigma = 1.166\bar{v}_{b,liq}^{1/3} = 1.166 \times 109.7^{1/3} = 5.582 \text{ Å}$$

The dimensionless temperature

$$\frac{k_b T}{\varepsilon} = \frac{T}{1.15T_b} = \frac{900}{1.15(136.4 + 273.15)} = 1.9108$$

can be used to find the collision integral from Table 7.3; the result is $\Omega_\mu = 1.1946$.

The viscosity can be obtained from eq. (7.154), i.e.,

$$\mu = 2.6693 \times 10^{-6} \frac{\sqrt{MT}}{\sigma^2 \Omega_\mu}$$

$$= 2.6693 \times 10^{-6} \times \frac{\sqrt{189.71 \times 900}}{5.582^2 \times 1.1946} = 2.96 \times 10^{-5} \text{ kg/s-m}$$

The gas constant of $TiCl_4$ is

$$R_g = \frac{R_u}{M} = \frac{8.3143 \times 10^3}{189.71} = 43.8 \text{J/kg-K}$$

The thermal conductivity of $TiCl_4$ can be obtained from eq. (7.161), i.e.,

$$k = \left(c_p + \frac{5}{4} R_g \right) \mu = \left(560.92 + \frac{5}{4} \times 43.8 \right) \times 2.96 \times 10^{-5} = 0.01826 \text{ W/m-K}$$

7.3.4 Typical Selected Applications

CVD in Horizontal Reactor

Since the susceptor in a horizontal reactor is heated from below, and the precursor flows along the horizontal direction, the temperature gradient in the precursor is perpendicular to the gas velocity. However, in this case, the forced convective boundary layer assumption is not valid, because the gas velocity is very low. In addition, Rayleigh-Bénard natural convection may occur on the susceptor because it is a nearly horizontal surface heated from below. Therefore, convection in a horizontal reactor is a mixed convection problem that combines the effects of forced and natural convection. The convection in the horizontal reactor is characterized by a low Reynolds number (under 50 based on channel height) and large temperature difference (400 to 1000 °C), which may lead to a complex flow structure and flow instability.

Chiu *et al.* (2000) observed the flow structures in a horizontal converging channel heated from below [see Fig. 7.15(a)]. The cross-section of the channel is

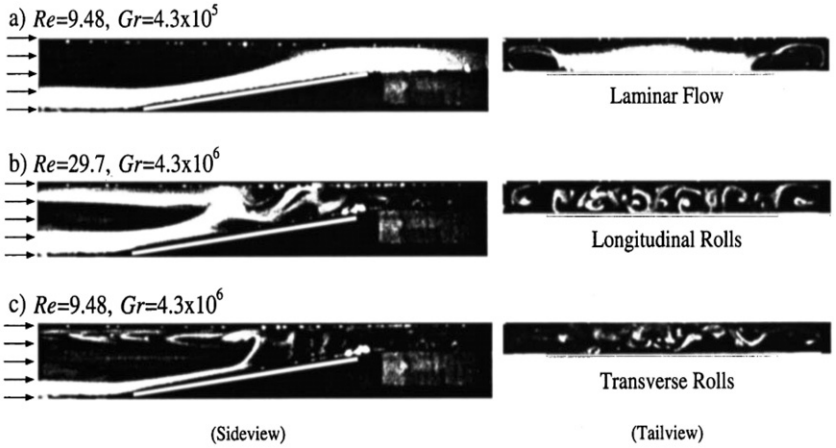

Figure 7.17 Side and tail views of flow patterns in a converging channel with 8° tilt [Reused with permission from Wilson K. S. Chiu *et al.*, *Physics of Fluids*, 12, 2128 (2000), Copyright 2000, American Institute of Physics].

25.4×5.08 cm (width×height: W×H) and the length of the channel is 91.4 cm. The length of the heated section, which can be tilted up to 10°, is 16.51 cm. They concluded that three flow regimes may exist, depending on Reynolds and Grashof numbers: (1) steady state laminar flow without roll, (2) longitudinal rolls, and (3) transverse rolls (see Fig. 7.17). The Reynolds number and Grashof number in Fig. 7.17 are defined as follows:

$$\mathrm{Re} = \frac{u_\infty H}{\nu} \tag{7.168}$$

$$\mathrm{Gr} = \frac{g\beta(q''H/k)H^3}{\nu^2} \tag{7.169}$$

where β is the coefficient of thermal expansion (1/K) and H is the height of the reactor.

The flow regime map obtained by Chiu *et al.* (2000) for a converging channel with 8° tilt is shown in Fig. 7.18. Steady-state laminar flow without roll exists when both the Reynolds number and the Grashof number are low. While longitudinal rolls are observed at a higher Reynolds number, transverse rolls occur at a higher Grashof number. The transition from longitudinal rolls to transverse rolls occurs at a critical mixed convection parameter of $\mathrm{Gr}/\mathrm{Re}^2 \approx 6000$.

The heat transfer of the converging channel heated from below is also investigated by Chiu *et al.* (2000), and the following empirical correlations are recommended:

$$\overline{\mathrm{Nu}} = 1.350\,\mathrm{Re}^{0.0531}\,\mathrm{Gr}^{0.0594}, \quad \text{for straight channel } (\theta = 0^\circ) \tag{7.170}$$

$$\overline{\mathrm{Nu}} = 2.398\,\mathrm{Re}^{0.0576}\,\mathrm{Gr}^{0.0192}, \quad \text{for converging channel } (\theta = 8^\circ) \tag{7.171}$$

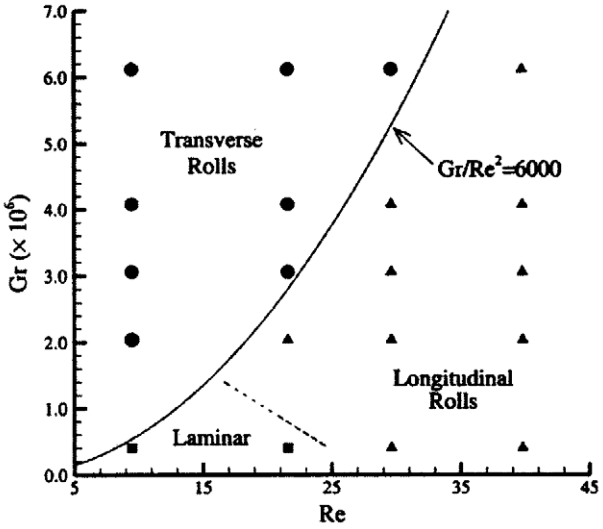

Figure 7.18 Flow regime map for a converging channel with 8° tilt [Reused with permission from Wilson K. S. Chiu *et al.*, *Physics of Fluids*, 12, 2128 (2000), Copyright 2000, American Institute of Physics].

where the average Nusselt number is defined as

$$\overline{\mathrm{Nu}} = \frac{q'' H}{k \Delta \bar{T}} \tag{7.172}$$

and $\Delta \bar{T}$ is the difference between the average temperature of the susceptor and the incoming temperature of the precursor.

There are also numerous efforts to model CVD in the horizontal reactors and detailed reviews are available in the literature (Jensen *et al.*, 1991; Mahajan, 1996). Some earlier studies adopted boundary-layer assumptions and neglect buoyancy, Soret, and Dufour effects, but Mahajan and Wei (1991) relaxed the boundary layer assumption and systematically studied the effects of buoyancy force, Soret, Dufour, and variable properties. The configuration as studied by Mahajan and Wei (1991) is shown in Fig. 7.15(a), in which the reactant, silane, and the carrier gas, hydrogen, enter the horizontal channel from the left and the CVD occurs on a susceptor tilted by θ. The monocrystalline silicon can be deposited on a susceptor as the result of chemical reaction.

The governing equations for the problem are eqs. (7.144) – (7.148) in the Cartesian coordinate system, with the Dufour heat flux as

$$\mathbf{q}'' = -k \nabla T + \alpha R_g T \frac{\bar{M}}{M_2} \mathbf{J}_1 \tag{7.173}$$

where $\bar{M}$ is the averaged molecular mass, M_2 is the molecular mass of the hydrogen, and $\mathbf{J}_1$ is the mass flux of reactant due to ordinary and thermal diffusions.

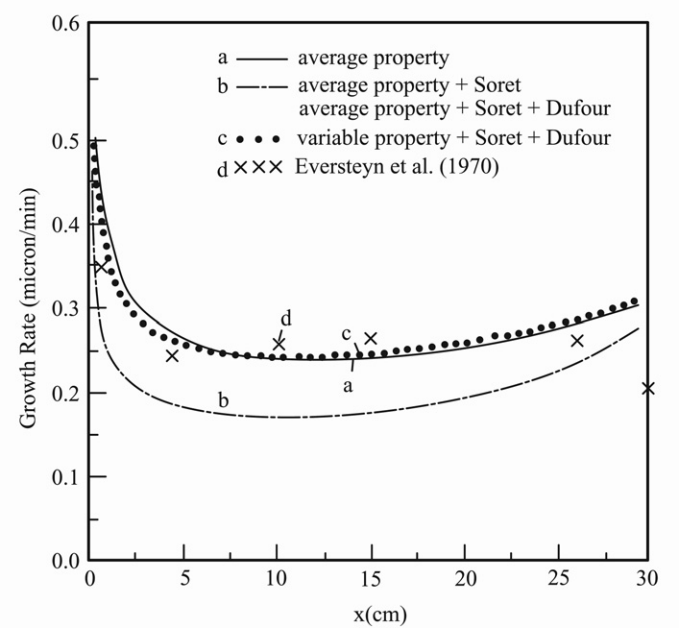

Figure 7.19 Growth rate of the silicon film grown obtained by different models (Mahajan, 1996; Reprinted with permission from Elsevier).

The deposition rate of the monocrystalline silicon can be obtained by

$$\dot{\mathbf{m}}_{\mathrm{Si}} = -\frac{M_{\mathrm{Si}} c D}{\rho_{\mathrm{Si}}} \nabla x_1 \big|_{\text{Susceptor Surface}} \tag{7.174}$$

where M_{Si} and ρ_{Si} are respectively molecular mass and density of silicon, c is molar concentration of the precursor, and x_1 is mole fraction of silane.

To compare the computational results with the experimental results by Eversteyn *et al.* (1970), Mahajan and Wei (1991) took the physical dimensions and the processing parameters were taken to be similar to those of Eversteyn *et al.* (1970): the height of the reactor was 2.05 cm, and the temperatures of the susceptor and the top wall were 1323 K and 300 K, respectively. The partial pressure of the carrier gas (hydrogen) and the reactant (silane) were 760 torr (1 atm) and 0.76 torr (0.001atm), respectively. The inlet velocity of the precursors was 0.175 m/s, and their temperature was 300 K.

Figure 7.19 shows comparison of the growth rates of the silicon in a horizontal reactor with a tilt angle of $\gamma = 2.9°$ obtained by different models, along with experimental data. It can be seen that curve *a*, with average properties and without Soret or Dufour effects, agreed with experimental results very well. When the Soret effect is included, the predicted deposit rate – represented by curve *b* – is significantly below the experimentally measured deposit rate. Addition of the Dufour effect did not improve the agreement with the experimental data. When variable properties are accounted for, the predicted

result – represented by curve *c* – again agreed with the experimental results. This interesting phenomenon indicates that the Dufour effect has very insignificant effect on the deposition rate, and the Soret effect and variable property effect can cancel each other. However, it is necessary to point out that the agreement of curve *a* and experimental results is coincidental, and the Soret and variable property effects should be included in the analysis.

CVD in Barrel Reactor

For large-volume production of epitaxial growth of the silicon, the barrel reactor shown in Fig. 7.15(c) is widely adopted. Transport phenomena in a barrel reactor are very complex and cannot be treated as axisymmetric (Curtis, 1976; Lord, 1987). The 3-D numerical model of transport phenomena in an idealized barrel reactor presented by Yang *et al.* (1992) will be introduced here. The physical model of the CVD reactor is shown in Fig. 7.20. The polygonal susceptor that is used in a barrel reactor is simplified as a circular cylindrical shape. The precursor gas that includes reactant silane and carrier-gas hydrogen enters two nozzles located on the top of the reactor at two different locations: θ = 0° and 180°. The precursors are induced into the reactor at an injection angle of ϕ. The flow is assumed to be laminar and the governing equations are eqs. (7.144) – (7.148) in the cylindrical coordinate system.

Yang *et al.* (1992) considered the following partial pyrolysis chemical reaction in the gas phase:

$$\mathrm{SiH_4(g) \rightarrow SiH_2(g)+H_2(g)} \tag{7.175}$$

with the following reaction rate:

$$\dot{m}'''_{\mathrm{SiH_2}} = -5\times10^{12}\,\rho\omega_{\mathrm{SiH_4}}\exp\left(-\frac{2.2\times10^{8}}{R_gT}\right) \tag{7.176}$$

The following two chemical reactions occurred on the surface of the susceptor:

$$\mathrm{SiH_4(g) \rightarrow Si(s)+2H_2(g)} \tag{7.177}$$

$$\mathrm{SiH_2(g) \rightarrow Si(s)+H_2(g)} \tag{7.178}$$

where the chemical reaction in eq. (7.177) was assumed to be kinetically controlled and eq. (7.178) is considered to be diffusion controlled. The rate of kinetically-controlled production of Si is obtained by

$$\dot{m}''_{\mathrm{Si}} = \frac{1}{M_{\mathrm{Si}}}\frac{k_1 p_{\mathrm{SiH_4}}}{1+k_2 p_{\mathrm{H_2}}+k_3 p_{\mathrm{SiH_4}}} \tag{7.179}$$

where $\mathrm{M_{Si}}$ is molecular mass of silicon, $k_1(\mathrm{mol\ Si/m^2\text{-}s}) = 1.25\times10^{9}e^{-18500/T}$, $k_2 = 1.75\times10^{3}(atm^{-1})$, $k_3 = 4\times10^{4}(atm^{-1})$, and $p_{\mathrm{H_2}}$ and $p_{\mathrm{SiH_2}}$ are the partial pressures of hydrogen and silane in atmospheric pressure. The temperature at the top surface of the reactor is assumed to be a linear profile, while the bottom

surface of the reactor is assumed to be adiabatic. The temperature of the susceptor stem is assumed to be maintained at the temperature of the inlet gas temperature so that there is no deposition on the stem. Other boundary conditions for velocity, temperature, and concentration are conventional.

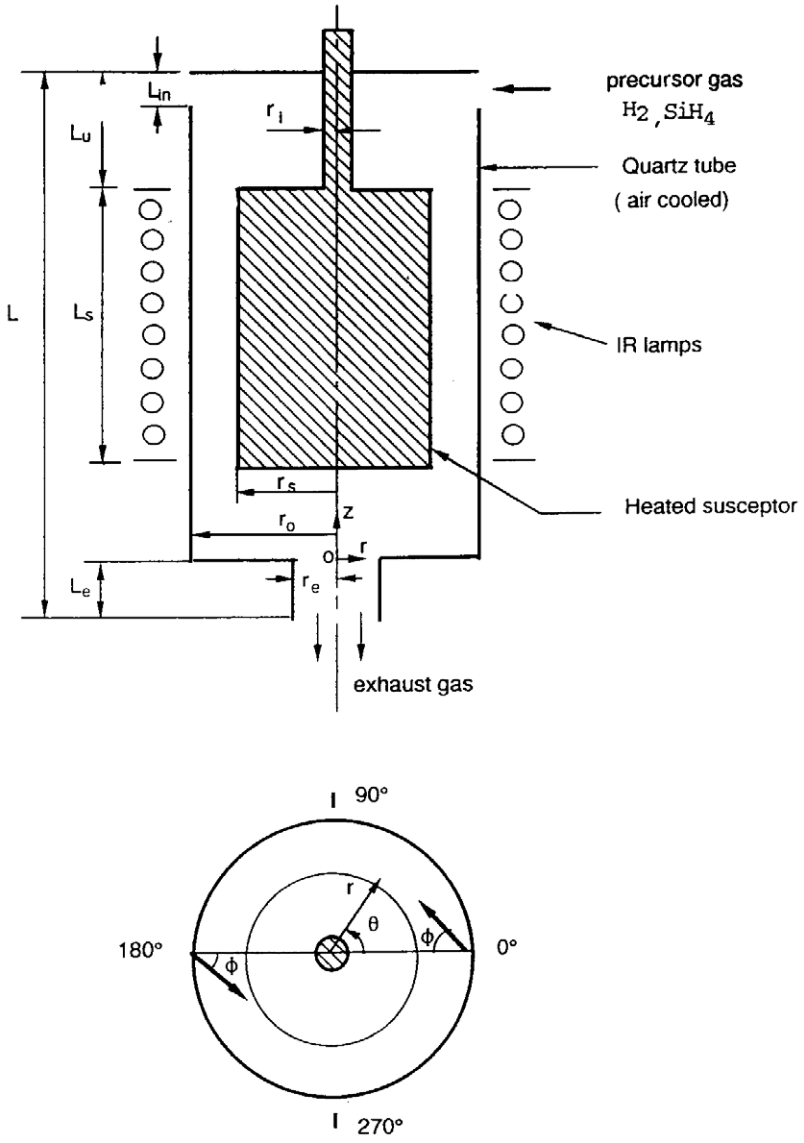

Figure 7.20 Idealized barrel CVD reactor (Yang *et al.*, 1992; Reproduced by permission of ECS – The Electrochemical Society).

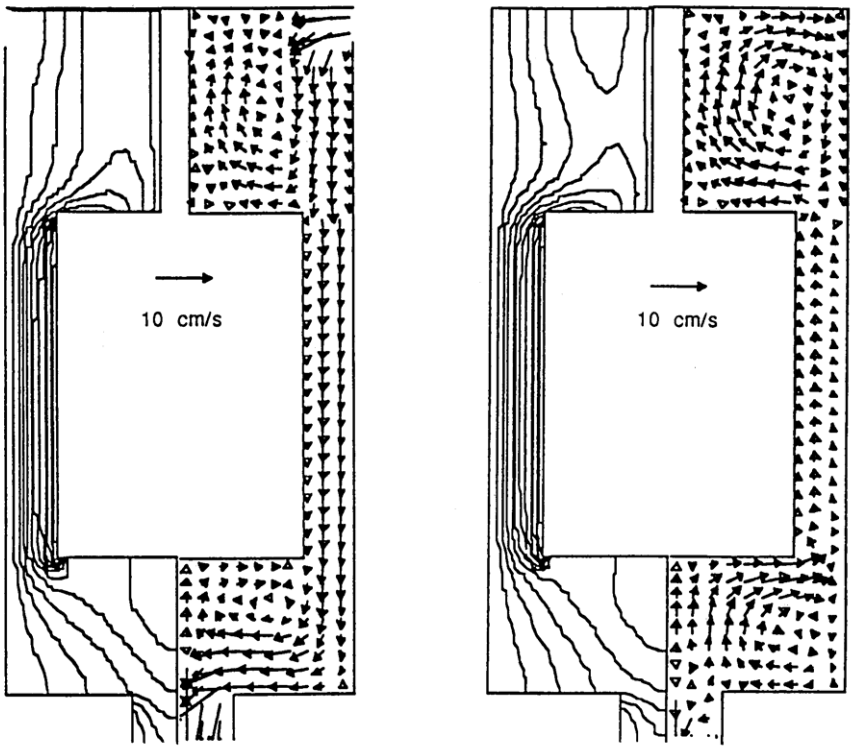

(a) $\theta = 0^{\circ}$ (b) $\theta = 90^{\circ}$

Figure 7.21 Temperature contour and flow fields at different planes (injection angle $\phi = 0^{\circ}$, susceptor rotation $\Omega = 0$ rpm ; Yang *et al.*, 1992; Reproduced by permission of ECS – The Electrochemical Society).

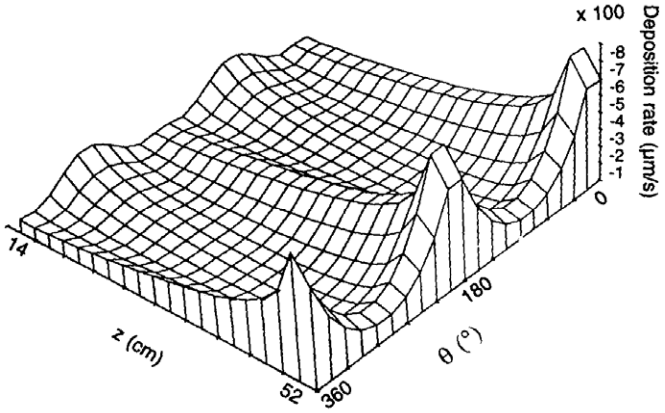

Figure 7.22 Deposition rate on the surface of the susceptor (Yang *et al*., 1992; Reproduced by permission of ECS – The Electrochemical Society).

Yang *et al.* (1992) obtained the numerical solution of the fluid flow, heat and mass transfer, and silicon deposition rate using the SIMPLE algorithm (Patankar, 1980); and the representative temperature and flow field are shown in Fig. 7.21. The dimensions of the reactors are: $L = 80$ cm, L_{in}=3.8 cm, L_u=22 cm, L_s=38 cm, L_e=6 cm, r_i=1 cm, r_s=15 cm, r_0=19 cm, and r_e=6 cm. The susceptor temperature is $T_s = 1300$ K, and the susceptor stem temperature is $T_i = 300$ K. The flow is very complex because the natural convection caused by a hot susceptor interacts with the forced convection induced by incoming injection flow. The distribution of the deposition rate shown in Fig. 7.22 indicates that the deposition rate varies significantly on the susceptor surface. The deposition rate is significantly higher at the location near the nozzles that induced the reactant than at other locations.

Laser Chemical Vapor Deposition (LCVD)

During LCVD, the spot on the substrate under laser irradiation is at a very high temperature (1200 K or higher). Temperature gradients in the source gases will cause natural convection in the chamber. The concentration of the gas mixture near the hot spot on the substrate is affected by the chemical reaction taking place on the substrate. Concentration differences in the chamber become another force driving natural convection in the chamber. For the case of LCVD by a stationary laser beam, Lee *et al.* (1995) concluded that the effect of natural convection on the thin film deposition rate was negligible and that the heat and mass transfer in the gases were dominated by diffusion. In the SALD process, a laser beam scans the substrate and induces chemical reaction; the resulting product forms a line on the substrate. These lines, formed by multiple laser scans, are subsequently interwoven to form a part layer. To thoroughly understand the effects of various physical phenomena – including natural convection – on the SALD process,

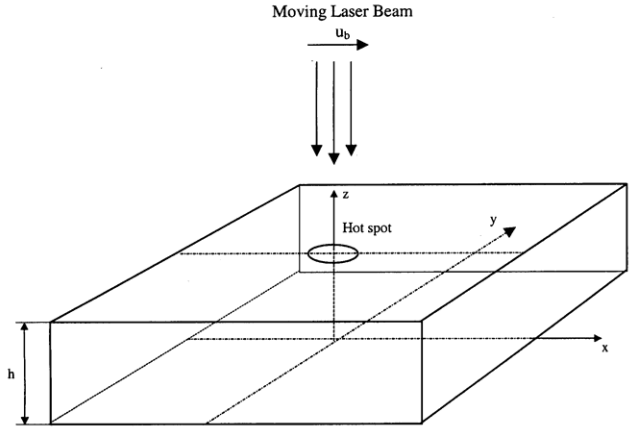

Figure 7.23 Physical model of Laser Chemical Vapor Deposition.

natural convection during LCVD with a moving laser beam was investigated by Zhang (2003).

The physical model of LCVD under consideration is illustrated in Fig. 7.23. A substrate made of Incoloy 800 with a thickness of h is located in the bottom of a chamber. Before the vapor deposition starts, the chamber is evacuated and then filled with a mixture of H_2, N_2, and $TiCl_4$. A laser beam moves along the surface of the substrate with a constant velocity, u_b. The initial temperature of the substrate, T_i, is below the chemical reaction temperature. Vapor deposition starts when the surface temperature reaches the chemical reaction temperature. The chemical reaction that occurs on the top substrate surface absorbs part of the laser energy and consumes the $TiCl_4$. A concentration difference is thereby established and becomes the driving force for mass transfer. The physical model of the LCVD process includes: natural convection, heat transfer in the substrate and gases, and chemical reaction, as well as mass transfer in the gases.

The laser beam travels with a constant velocity u_b along the surface of the substrate, constituting a typical moving heat source problem. If the substrate is sufficiently large in comparison to the diameter of the laser beam, which has an order of magnitude of 10^{-3} m, a quasi-steady state occurs. The system appears to be in steady-state from the standpoint of an observer located in and traveling with the laser beam. By simulating LCVD with a moving laser beam in the moving coordinate system, the computational time will be substantially shortened, thereby enabling numerical simulation for a significant number of cases.

Heat transfer in the substrate and gases is modeled as one problem with different thermal properties in each region. In the substrate region, the velocity is set to zero in the numerical solution. The advantage of modeling the heat and mass transfer in the substrate and the gases as one problem is that the temperature distribution in the substrate and gases can be obtained by solving one equation. This eliminates the iteration procedure needed to match the boundary condition at the substrate-gas interface. Since the model geometry is symmetric about the xz plane, only half of the problem needs to be investigated. For a coordinate system moving with the laser beam, as shown in Fig. 7.23, the laser beam is stationary but the substrate and the chamber move with a velocity $-u_b$. The heat and mass transfer in the substrate and gases is governed by eqs. (7.144)– (7.148), with buoyancy forces due to temperature and concentration gradients accounted for, but the Soret effect neglected (Zhang, 2003). For the substrate region, the thermal properties are those of Incoloy 800, the substrate material. For the gaseous region, the thermal properties are determined by the individual thermal properties of H_2, N_2, and $TiCl_4$ as well as their molar fractions [see eq. (7.160) – (7.161)]. The mass diffusivity of $TiCl_4$ in the gas mixture is determined by the Stefan-Maxwell equation, using the binary diffusivity of $TiCl_4$ with respect to all other species, which is calculated using the hard sphere model.

The heat flux at the substrate surface due to laser beam irradiation and chemical reaction is expressed as

$$q'' = \frac{2P\alpha_a}{\pi r_0^2}\exp\left[-\frac{2(x^2+y^2)}{r_0^2}\right] - \varepsilon\sigma(T^4 - T_\infty^4) + \rho_{TiN}\Delta H_R u_b \frac{d\delta}{dx}, \quad z = h \tag{7.180}$$

where ΔH_R is chemical reaction heat, and $d\delta/dt$ is the deposition rate. For a chemical reaction in the order of unity, the deposition rate is expressed as

$$\frac{d\delta}{dx} = -\frac{\gamma_{TiN}K_0}{u_b\rho_{TIN}}\exp\left(-\frac{E}{R_u T_s}\right)\omega_s \tag{7.181}$$

where ω_s represents the concentration of $TiCl_4$ at the surface of the substrate. The constant K_0 in eq. (7.181) is defined as $K_0 = (\omega_{H_2})_i(\omega_{N_2})_i^{1/2}K_0'$.

The coefficient γ_{TiN} in eq. (7.181) is a sticking coefficient defined as

$$\gamma_{TiN} = \begin{cases} 1 & T < T_m \\ 1 + (T_m - T_s)/(T_M - T) & T_m \le T \le T_M \\ 0 & T > T_M \end{cases} \tag{7.182}$$

where T_s is the surface temperature of the substrate, T_m is a threshold temperature below which the product of the chemical reaction can fully stick to the substrate, and T_M is another threshold temperature above which no product of chemical reaction can be stuck on the substrate. If the surface temperature is between T_m and T_M, the product of chemical reaction can only be partially stuck on the substrate. The values of T_m and T_M are chosen as 1473 K and 1640 K, respectively (Conde *et al.*, 1992).

The boundary conditions of the velocities are

$$u = -u_b, \quad v = w = 0, \quad |x| \to \infty \tag{7.183}$$

$$v = \frac{\partial u}{\partial y} = \frac{\partial w}{\partial y} = 0, \quad y = 0 \tag{7.184}$$

$$u = -u_b, \quad v = w = 0, \quad y \to \infty \tag{7.185}$$

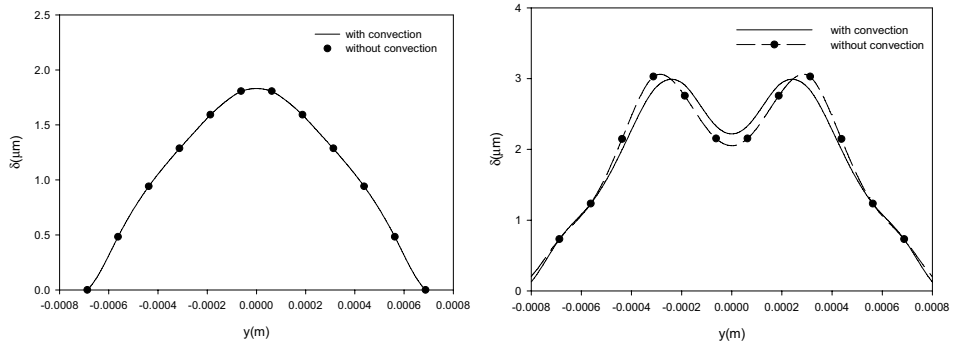

(a) P=300W, u_b=1.2mm/s (b) P=360W, u_b=1.2mm/s

Figure 7.24 Comparison of cross-sections (Zhang, 2003).

$$u = -u_b, \quad v = w = 0, \quad z = 0, \infty \tag{7.186}$$

The governing equations are discretized using the finite volume method (Patankar 1980); the SIMPLEC algorithm (Van Doormaal and Raithby, 1984) was employed to handle the linkage between velocity and pressure. The results show that the effect of natural convection on the shape of deposited film is negligible for the laser power of P = 300 W [see Fig. 7. 24(a)]. When the laser power is increased to 360W, the effect of natural convection on the shape of the cross-section becomes important, although the cross sectional area is almost unchanged [see Fig. 7.24(b)]. A groove is observed on the top of the deposited film for P = 360 W due to a low sticking coefficient.

Zhang (2004) presented a parametric study on shape and cross-sectional area of the thin film produced by LCVD with a moving laser beam. The effect of natural convection on the LCVD process is neglected because it has little effect on the shapes of deposited film, and it has no effect on the cross-sectional area of the thin film. The effects of laser scanning velocity, laser power, and radius of the laser beam on the shapes of the deposited film were investigated. The results showed that a groove could be observed on the top of the film in conjunction with higher laser power and lower scanning velocity. The cross-sectional area, calculated by

$$A_c = \frac{2}{r_0^2} \int_0^\infty \delta dy \tag{7.187}$$

at different processing parameters, is shown in Fig. 7.25. It decreases with increasing scanning velocity. It also increases with increasing laser power and decreasing laser beam radius. The following empirical correlation on the dimensionless cross-sectional area is obtained (Zhang, 2004):

$$A_c = a_0 + a_1 \left(\frac{Bi}{Pe} \right)^{1.35} \tag{7.188}$$

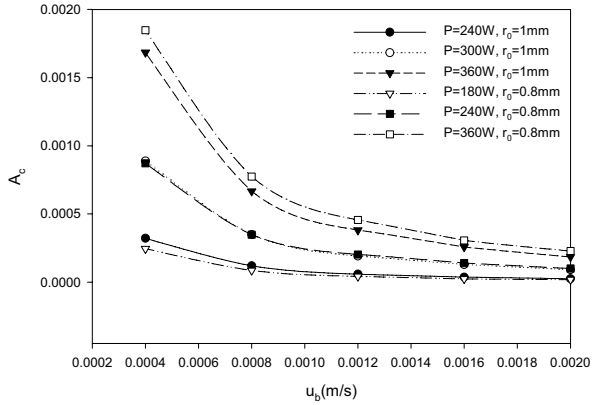

Figure 7.25 Dimensionless cross-sectional area vs. scanning velocity (Zhang, 2004).

where

$$a_0 = \begin{cases} -2.136\times10^{-5} + 6.126\times10^{-6}\,\mathrm{Bi} & r_0 = 1.0 \text{ mm} \\ -9.206\times10^{-5} + 9.352\times10^{-5}\,\mathrm{Bi} & r_0 = 0.8 \text{ mm} \end{cases} \tag{7.189}$$

$$a_1 = \begin{cases} 8.343\times10^{-7} + 1.423\times10^{-5}\,\mathrm{Bi} & r_0 = 1.0 \text{ mm} \\ -2.587\times10^{-5} + 4.372\times10^{-5}\,\mathrm{Bi} & r_0 = 0.8 \text{ mm} \end{cases} \tag{7.190}$$

The Biot number and Peclet number are defined as

$$\mathrm{Bi} = \frac{\alpha_a P}{\pi r_0 k_s (T_c - T_i)} \tag{7.191}$$

$$\mathrm{Pe} = \frac{u_b r_0}{\alpha_s} \tag{7.192}$$

where α_a is the absorptivity of the laser beam on the substrate surface, P is the laser power, r_0 is the radius of the laser beam, T_c is the chemical reaction temperature, T_i is the initial temperature of the gases, and u_b is the laser scanning velocity. The thermal conductivity k_s and the thermal diffusivity α_s in eqs. (7.191) – (7.192) are those of the substrate (Incoloy) at chemical reaction temperature.

References

Bauerle, D., 1996, *Laser Processing and Chemistry,* Springer, New York, NY.

Bird, R.B., Stewart, W.E., and Lightfoot, E.N., 2002, *Transport Phenomena*, 2nd ed., John Wiley and Sons, New York.

Chiu, W.K.S., Richards, C.J., and Jaluria, Y., 2000, "Flow Structure and Heat Transfer in a Horizontal Converging Channel Heated from Below," *Physics of Fluids*, Vol. 12, pp. 2128-2136.

Conde, O., Kar, A., and Mazumder, J., 1992, "Laser Chemical Vapor Deposition of TiN Dot: A Comparison of Theoretical and Experimental Results," *Journal of Applied Physics,* Vol. 72, pp. 754-761.

Curtis, B.J., 1976, "Temperature Asymmetries and Fluctuation in a Barrel Reactor," *Journal of the Electrochemical Society*, Vol. 123, pp. 437-439.

Eckert, E.R.G., and Goldstein, R.J., 1976, *Measurement in Heat Transfer*, McGraw-Hill, New York, NY.

Elyukhin, V.A., Garcia-Salgado, G., and Pena-Sierra, R., 2002, "Thermodynamic Model for Low Temperature Metalorganic Chemical Vapor Deposition of GaN," *Journal of Applied Physics*, Vol. 91, pp. 9091-9094.

Evans, G., and Greif, R., 1987, "A Numerical Model of the Flow and Heat Transfer in a Rotating Disk Chemical Vapor Deposition Reactor," ASME *Journal of Heat Transfer,* Vol. 109, pp. 928-935.

Eversteyn, F.C., Severin, P.I.W., vida Brekel, C.H.J., and Peck, H.L., 1970, "A Stagnation Layer Model for the Epitaxial Growth of Silicon from Silane in a Horizontal Reactor," *Journal of* the *Electrochemistry Society*, Vol. 117, pp. 925-931.

Glassman, I., 1987, *Combustion,* 2nd ed., Academic Press, Orlando, FL.

Herring, R.B., 1990, "Silicon Epitaxy," In *Handbook of Semiconductor Silicon Technology*, edited by O'Mara, W.C., Herring, R.B., and Hunt, L.P., Noyes Publications, Park Ridge, NJ, pp. 258-336.

Jakubenas, K.J., Birmingham, B., Harrison, S., Crocker, J., Shaarawi, M.S., Tompkins, J.V., Sanchez, J., and Marcus, H.L., 1997, "Recent Development in SALD and SALDVI," *Proceedings of 7th International Conference on Rapid Prototyping*, San Francisco, CA.

Jensen, K.F., Einset, E.O., and Fotiadis, D.I., 1991, "Flow Phenomena in Chemical Vapor Deposition of Thin Films," *Annu. Rew. Fluid Mech.*, Vol. 23, pp. 197-232.

Kaviany, M, 2001, *Principles of Convective Heat Transfer,* 2nd ed., Springer Verlag, New York.

Kays, W.M., Crawford, M.E., and Weigand, B., 2004, *Convective Heat Transfer*, 4th ed., McGraw-Hill, New York, NY.

Kurosaki, Y., 1973, "Coupled Heat and Mass Transfer in a Flow between Parallel Flat Plate (Uniform Heat Flux)," *Journal of* the *Japan Society of Mechanical Engineers*, Part B, Vol. 39, pp. 2512-2521 (in Japanese).

Kurosaki, Y., 1974, "Coupled Heat-Mass Transfer of a Flat Plate with Uniform Heat Flux in a Laminar Parallel Flow," *Journal of* the *Japan Society of Mechanical Engineers*, Part B, Vol. 40, pp. 1066-1072 (in Japanese).

Kwok, K.H., and Chiu, W.K.S., 2003, "Deposition Rate and Temperature of Carbon Films during Laser-Induced CVD on a Moving Substrate," *Carbon,* Vol. 41, pp. 2295-2305.

Lee, Y.L., Tompkins, J.V., Sanchez, J.M., and Marcus, H.L., 1995, "Deposition Rate of Silicon Carbide by Selected Area Laser Deposition," *Proceedings of Solid Freeform Fabrication Symposium 1995*, pp. 433-439.

Lord, H.A., 1987, "Convective Transport in Silicon Epitaxial Deposition in a Barrel Reactor," *Journal of* the *Electrochemical Society*, Vol. 134, pp. 1227-1234.

Mahajan, R.L., 1996, "Transport Phenomena in Chemical Vapor-Deposition Systems," *Advances in Heat Transfer*, Academic Press, San Diego, CA.

Mahajan, R.L., and Wei, C., 1991, "Buoyancy, Soret, Dufour, and Variable Property in Silicon Epitaxy," ASME *Journal of Heat Transfer*, Vol. 113, p. 688-695.

Marcus, H.L, Zong, G., and Subramanian, P.K., 1993, "Residual Stresses in Laser Processed Solid Freeform Fabrication, Residual Stresses in Composites," *Measurement, Modeling and Effect on Thermomechanical Properties*, Barrera, E.V. and Dutta, I., eds., TMS, pp. 257-271.

Mazumder, J., and Kar, A., 1995, Th*eory and Application of Laser Chemical Vapor Deposition*, Plenum Publishing Co., New York, NY.

Patankar, S.V., 1980, *Numerical Heat Transfer and Fluid Flow*, Hemisphere, Washington, DC.

Powell, C., Blocher, M., and Oxley, J., 1966, *Vapor Deposition*, John Wiley and Sons, New York.

Seshan, K. ed., 2001, *Handbook of* Th*in Film Deposition Techniques: Principles, Me*th*ods, Equipment and Applications,* 2nd edition, Noyes Publications, Princeton, NJ.

Sivaram, S., 1995, *Chemical Vapor Deposition:* Th*ermal and Plasma Deposition of Electronic Materials*, Kluwer Academic Publishers, Bordrecht, Netherlands.

Sun, L., Jakubenas, K.J., Crocker, J.E., Harrison, S., Shaw, L.L., and Marcus, H.L., 1998, "In Situ Thermocouples in Micro-Components Fabricated Using SALD/SALDVI Techniques: II Evaluation of Processing Parameters," *Materials and Manufacturing Processes*, Vol. 13, pp. 883-907.

Taylor, C.A., Wayne, M.F., and Chiu, W.K.S., 2004, "Microstructural Characterization of Thin Carbon Films Deposited from Hydrocarbon Mixtures," *Surface and Coatings Technology,* Vol. 182, pp. 131-137.

Ueda, O., 1996, *Reliability and Degradation of III-V Optical Devices*, Artech House, Inc., Boston.

Van Doormaal, J.P., and Raithby, G.D., 1984, "Enhancements of the Simple Method For Predicting Incompressible Fluid Flows," *Numerical Heat Transfer*, Vol. **7**, pp. 147-163.

Versteeg, V.A., Avedisian, C.T., and Raj, R., 1995, "Metalorganic Chemical Vapor Deposition by Pulsed Liquid Injection Using an Ultrasonic Nozzle: Titanium Dioxide on Sapphire from Titanium (IV) Isopropoxide," *Journal of* th*e American Ceramic Society*, Vol. 78, pp. 2763-2768. .

Yang, L., Farouk, B., and Mahajan, R.L., 1992, "Three-Dimensional Predictions of Silicon Deposition in a Barrel Type CVD Reactor," *Journal of* th*e Electrochemical Society*, Vol. 159, pp. 2666-2673.

Zhang, Y., 2002, "Coupled Forced Convective Heat and Mass Transfer in a Circular Tube with External Convective Heating," *Progress of Computational Fluid Dynamics Journal,* Vol. 2, pp. 90-96.

Zhang, Y., 2003, "Quasi-Steady State Natural Convection in Laser Chemical Vapor Deposition with a Moving Laser Beam," ASME *Journal of Heat Transfer*, Vol. 125, No. 3, pp. 429-437.

Zhang, Y., 2004, "A Simulation-Based Correlation of Cross-Sectional Area of the Thin Film Produced by Laser Chemical Vapor Deposition with a Moving Laser Beam," ASME *Journal of Manufacturing Science and Engineering,* Vol. 126, No. 4, pp. 796-800.

Zhang, Y., and Chen, Z.Q., 1990, "Analytical Solution of Coupled Laminar Heat-Mass Transfer inside a Tube with Adiabatic External Wall," *Proceedings of* the *3rd National Interuniversity Conference on Engineering* Th*ermophysics*, Xi'an Jiaotong University Press, Xi'an, China, pp. 341-345.

Zhang, Y., and Chen, Z.Q., 1992, "Analytical Solution of Coupled Laminar Heat- Mass Transfer in a Tube with Uniform Heat Flux," *Journal of Thermal Science*, Vol. 1, No. 3, pp. 184-188.

Zhang, Y., Chen, Z.Q., and Chen, M., 1996, "Local Non-Similarity Solution of Coupled Heat-Mass Transfer of a Flat Plate with Uniform Heat Flux in a Laminar Parallel Flow," *Journal of Thermal Science*, Vol. 5, No. 2, pp. 112-116.

Zhang, Y., and Faghri, A., 2000, "Thermal Modeling of Selective Area Laser Deposition of Titanium Nitride on a Finite Slab with Stationary and Moving Laser Beams," *International Journal of Heat and Mass Transfer*, Vol. 43, pp. 3835-3846.

Problems

7.1. A subcooled solid is exposed to its superheated vapor as shown in Fig. 7.2(a). The temperature at the left surface of the solid is T_0, which is below the interfacial temperature. Depending on the direction of the overall heat flux at the interface, both sublimation and deposition are possible. Derive the criteria for sublimation and deposition.

7.2. Superheated vapor is brought into contact with a cold surface at a temperature of T_0, and deposition takes place on the cold surface. Find the deposition rate by solving transient conduction in the deposited solid phase.

7.3. For sublimation inside a circular tube subject to constant heat flux heating (see Section 7.2.2), show that the dimensionless mean temperature and concentration are related by $\theta_m + \varphi_m - \varphi_0 = 4\xi$.

7.4. Show that the fully developed dimensionless temperature and mass fraction distributions for sublimation inside a circular tube subject to constant heat flux heating discussed in Section 7.2.2 are eqs. (7.94) and (7.95).

7.5. The inner surface of a circular tube with radius R is coated with a layer of sublimable material, and the outer wall of the tube is kept at a constant temperature T_w. The fully developed gas enters the tube with a uniform inlet mass fraction of the sublimable substance ω_0 that equals the saturation mass fraction corresponding to the inlet temperature T_0. The thermal and mass diffusivities are assumed to be the same, i.e., Le = 1. Find the local Nusselt number based on convective heat flux and the total heat flux at the wall, and the local Sherwood number.

7.6. Obtain the fully developed Nusselt number based on convective heat flux and the total heat flux at the wall, and the local Sherwood number for the sublimation problem discussed in Example 5.1.

7.7. A gas with a velocity of u_∞, a concentration of a sublimable substance, ω_∞, and a temperature of T_∞ flows parallel to a flat plate coated with sublimable materials; the back of the flat plate is adiabatic (see Fig. P7.1). Specify the governing equations and the corresponding boundary conditions of the sublimation problem.

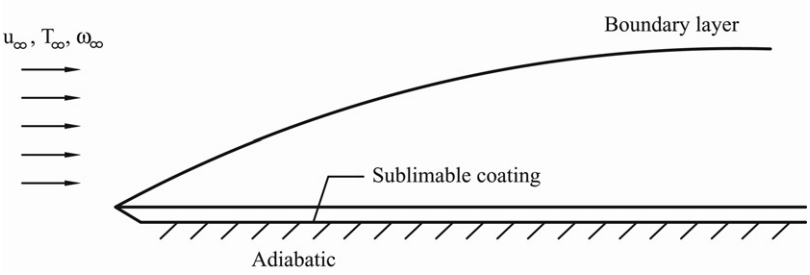

Fig. P7.1

7.8. Suppose the blowing velocity on the surface of the flat plate satisfies $v_w \propto x^{-1/2}$. Introduce appropriate similarity variables to the governing equations in Problem 7.7 and reduce the governing equations into a set of ordinary differential equations.

7.9. Write a computer program to solve for the ordinary differential equations of Problem 7.8, and obtain the local Nusselt number and Sherwood number.

7.10. Air with a temperature of 27 °C flows at 1 m/s over a 1 m-long solid fuel surface at a temperature of 527 °C. The average blowing velocity due to sublimation of the solid fuel is 0.01 m/s, and the heat released per unit mass of the oxidant consumed is 10,000 kJ/kg. The latent heat of sublimation for the solid fuel is 1350 kJ/kg. The sensible heat required to raise the surface temperature of the solid fuel to sublimation temperature, and heat loss to the solid fuel, can be neglected. Estimate the mass fraction of the oxidant at the solid fuel surface.

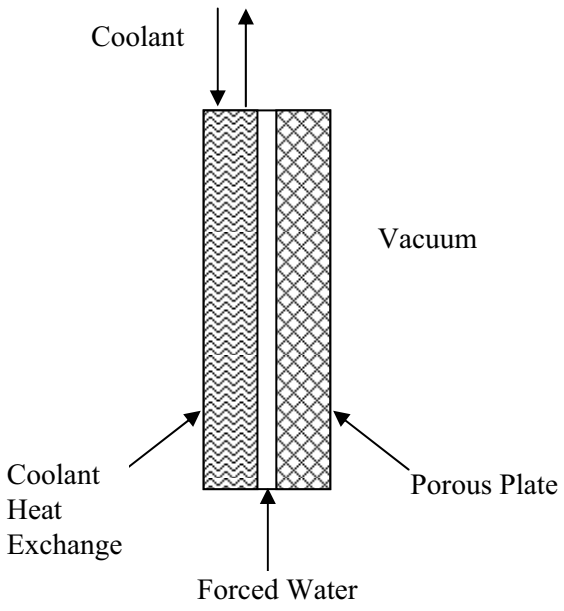

Figure P7.2

7.11. Manned spacecraft and spacesuits reject excess thermal energy by sublimating water into the vacuum of space. The sublimator consists of a porous plate exposed to vacuum on one side and feed water on the other side. The feed water seeps into the porous plate, where it then freezes. In Fig. P7.2, the sublimator also has a separate coolant heat exchanger that interfaces with the feed water. Describe in detail how the process of sublimation keeps the astronaut or spacecraft cool.

7.12. The precursor for SALD of TiN film is a mixture of titanium tetrachloride, nitrogen, and hydrogen (Conde *et al.*, 1992). The total pressure in the chamber is 207 torr and the partial pressure of titanium tetrachloride is 7 torr. The partial pressures of N_2 and H_2 are the same. Estimate the viscosity and thermal conductivity of the precursors at 900 K.

7.13. Estimate the binary mass diffusivity of titanium tetrachloride to nitrogen gas in the gaseous mixture described in Problem 7.11. The collision diameter of a nitrogen molecule is $\sigma = 3.681\,\text{Å}$ and the characteristic energy of interaction between molecules satisfies $\varepsilon / k_b = 91.5$ K.

7.14. What is the binary mass diffusivity of titanium tetrachloride to the hydrogen gas in the gaseous mixture described in Problem 7.11? The collision diameter of the hydrogen molecule is $\sigma = 2.915\,\text{Å}$ and the characteristic energy of interaction between hydrogen molecules satisfies $\varepsilon / k_b = 38.0$ K.

7.15. Find the mass diffusivity of $TiCl_4$ to a mixture of N_2 and H_2 used in SALD of TiN. The total pressure of the precursors is 207 torr, and the partial pressure of $TiCl_4$ is 7 torr. The partial pressures of both N_2 and H_2 are at 100 torr.

7.16. In a horizontal CVD reactor, the height of the converging channel is 5.08 cm and the susceptor is tilted by 8°. The surface heat flux at the susceptor is 50 W/m^2 and the properties of the precursors can be taken as those of air at 300 K. The incoming velocity of the precursors is 1 cm/s. What is the flow pattern in the converging channel?

7.17. If the incoming temperature of the precursors in Problem 7.15 is 300 K, find the average surface temperature of the susceptor.

7.18. The threshold temperature of the chemical reaction taking place in a horizontal reactor is 350 K. The height of the reactor is 5.08 cm and the susceptor is flat ($\theta = 0^\circ$). The precursors at 300 K enter the horizontal reactor with a low velocity of 3mm/s. What is the required heat flux at the susceptor surface?

7.19. In an LCVD of TiN using a mixture of $TiCl_4$, N_2, and H_2, a laser beam with a power of 350W and a radius of 1 mm scans at a velocity of 1.5 mm/s. The absorptivity of the laser beam on the substrate surface is 0.23. The initial gas temperature is 338K and the chemical reaction temperature is 1173 K. The thermal conductivity and thermal diffusivity of the substrate at 1173 K are 24.5 W/m-K and 4.677×10^{-6} m^2/s, respectively. Estimate the dimensional cross-sectional area of the deposited film.

7.20. Model a simplified catalytic reaction in Fig. P7.3 in which gas A enters the reactor and is convected to B. Assume that at the bottom surface a reaction 2A→B is being carried out steadily, irreversibly, and instantaneously in an isothermal process. Assume ideal gas and obtain the local mass flux rate of A to B.

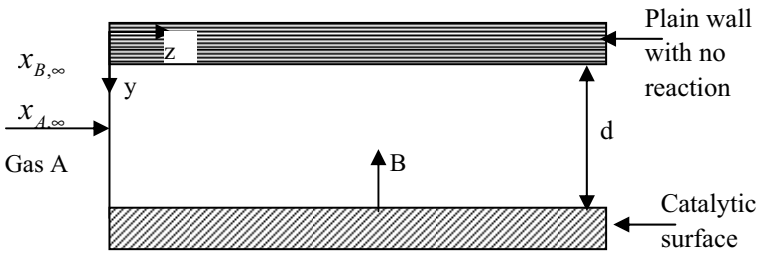

Figure P7.3

7.21. Repeat Problem 7.20, but account for the finite reaction kinetics at the catalytic surface. All other assumptions remain the same. Assume the rate at which A disappears at the catalyst surface is proportional to the molar concentration of A in the gas at the surface (first order surface reaction).